Stochastic Receding Horizon Control of Active Distribution Networks With Distributed Renewables

Yibao Jiang, Can Wan, *Member, IEEE*, Jianhui Wang, *Senior Member, IEEE*, Yonghua Song, *Fellow, IEEE*, and Zhao Yang Dong, *Fellow, IEEE*

***Abstract*—High penetration of distributed renewable energy introduces significant uncertainties to active distribution networks. Optimal control methods accounting for inherent uncertainties are needed to facilitate economic and reliable operation of active distribution networks. This paper proposes a stochastic receding horizon control method based on modified stochastic model predictive control framework to integrate high penetration of distributed generation. Multiple controllable resources are jointly optimized over a finite prediction horizon while ensuring relevant security restrictions. The simplified Z-bus sensitivity for active distribution networks is developed for computationally efficient estimation of system nonlinearity with high accuracy, and is combined with the sequential linear programming to iteratively derive the linear state space model for compensation of cumulative modeling errors. Furthermore, the voltage limitations are reformulated as chance constraints to indicate the probabilistic reliability index of voltage qualification rate, and achieve tradeoffs between cost reduction and voltage regulation. The affine-disturbance feedback control policy is leveraged here to enforce close-loop control performance and analytically transform intractable chance constraints into second-order cone constraints. Comprehensive case studies based on 33-bus and 123-bus distribution systems are carried out to demonstrate the capability and effectiveness of the proposed approach in terms of modeling accuracy, control performance, cost reduction, and method scalability. The proposed approach can effectively enforce voltage regulation against uncertainties with the prescribed probability level. Control costs and constraint violation can be reduced compared with deterministic model predictive control and open-loop control strategies.**

***Index Terms*—Active distribution network, stochastic model predictive control, uncertainty, chance constraint, distributed renewable generation.**

Manuscript received March 19, 2018; revised July 19, 2018 and October 10, 2018; accepted October 21, 2018. Date of publication November 2, 2018; date of current version February 18, 2019. This work was supported in part by the National Key R&D Program of China under Grant 2018YFB0905000, in part by the National Natural Science Foundation of China under Grants 51877189 and 51761135015, and in part by the Fundamental Research Funds for the Central Universities under Grant 2018QNA4015. The work of C. Wan was supported by the Hundred Talents Program of Zhejiang University. Paper no. TPWRS-00399-2018. *(Corresponding author: Can Wan.)*

Y. Jiang and C. Wan are with the College of Electrical Engineering, Zhejiang University, Hangzhou 310027, China (e-mail: canwan@zju.edu.cn).

J. Wang is with the Department of Electrical Engineering, Southern Methodist University, Dallas, TX 75275 USA.

Y. Song is with the Department of Electrical and Computer Engineering, University of Macau, Taipa, Macau, China, and also with the College of Electrical Engineering, Zhejiang University, Hangzhou 310027, China.

Z. Y. Dong is with the School of Electrical Engineering and Telecommunications, University of New South Wales, Sydney, NSW 2052, Australia.

Color versions of one or more of the figures in this paper are available online at http://ieeexplore.ieee.org.

Digital Object Identifier 10.1109/TPWRS.2018.2879451

NOMENCLATURE

The main notations of this paper are list below.

A. Abbreviations

ADN, SU	Active distribution network, storage unit.
SSC, DG	Switchable shunt capacitor, distributed generator.
OLTC	On load tap changing transformer.
PV, WT	Photovoltaic, wind turbine.
MPC, SSM	Model predictive control, state space model.
SMPC	Stochastic model predictive control.
SLP	Sequential linear programming.
DMPC	Deterministic model predictive control.
SMPC-HC	Stochastic model predictive control with hard constraints.
SRHC	Stochastic receding horizon control.
PBC, OLC	Perfect bound control, open-loop control.
MOV	Minimal objective value.
SSVD	Steady-state voltage deviation.

B. Indices and Sets

$\mathcal{I}^{\mathrm{PV}}, \mathcal{I}^{\mathrm{WT}}$	Sets of buses with PVs and WTs.
$\mathcal{I}^{\mathrm{L}}$	Sets of buses with loads.
$\mathcal{I}^{\mathrm{cDG}}, \mathcal{I}^{\mathrm{SU}}$	Sets of buses with controllable DGs and SUs.
$\mathcal{I}^{\mathrm{C}}, \mathcal{I}^{\mathrm{OLTC}}$	Set of buses with SSCs and OLTCs.
$\mathcal{I}^{\mathrm{IN}}$	Set of buses without the slack node.
$\mathcal{T}$	Set of prediction horizon.
$\mathcal{M}, m$	Set of controllable DGs, controllable DG index.
$\mathcal{S}, s$	Set of SUs, SU index.
$\mathcal{C}, c$	Set of SSCs, SSC index.
$\mathcal{O}, o$	Set of OLTCs, OLTC index.

C. Decision Variables

$P_i^{\mathrm{cDG}}, Q_i^{\mathrm{cDG}}$	Active/reactive power (MW/MVar) of the controllable DG at bus i.
$P_i^{\mathrm{d,SU}}, P_i^{\mathrm{c,SU}}$	Discharging/charging power (MW) of the SU at bus i.
$v_i^{\mathrm{d,SU}}, v_i^{\mathrm{c,SU}}$	Discharging/charging states of the SU at bus i.
SoC_i^{SU}	State of charge (%) of the SU at bus i.
$Q_i^{\mathrm{C}}, \Delta Q_i^{\mathrm{C}}$	Reactive power (MVar) and reactive ramping power (MVar) of the SSC at bus i.
N_i^{C}	Integer number of connected capacitor banks of the SSC at bus i.
t_{ij}^{OLTC}	OLTC tap position between buses i and j.
$\Delta t_{ij}^{\mathrm{OLTC}}$	Change step of tap positions of the OLTC placed between buses i and j.

k_{ij} Ratio of the OLTC between buses i and j.
k_{ij}^{tap} Relative ratio of the OLTC placed between bus i and bus j related to tap changing.
$\boldsymbol{x}$ State vector representing voltage magnitudes of all buses measured in pu.
$\boldsymbol{u}$ Control vector denoting power setpoints of controllable DGs, SSCs, SUs, and tap positions of OLTCs.
$\boldsymbol{\Delta u}$ Adjustments of active and reactive power of controllable DGs, active power of SUs, reactive power of SSCs, and tap regulations of OLTCs.
D_i^{SU} Depth of discharge (%) of the SU at bus i.
N_i^{SU} Number of remaining cycles of the SU at bus i.
$P_i^{\text{CP}}, Q_i^{\text{CP}}$ Active/reactive power (MW/MVar) from the main grid at bus i.
$P_{\text{loss}}, Q_{\text{loss}}$ Active/reactive power losses (MW/MVar).
$\Delta P_i^{\text{cDG}}, \Delta Q_i^{\text{cDG}}$ Active/reactive ramping power (MW/MVar) of the controllable DG at bus i.
$\Delta P_i^{\text{d,SU}}, \Delta P_i^{\text{c,SU}}$ Discharging/charging ramping power (MW) of the SU at bus i.

D. Disturbance Variables

$\boldsymbol{\Delta d}$ External disturbances of PVs, WTs and loads.
$P_i^{\text{PV}}, Q_i^{\text{PV}}$ Active/reactive power injections of the PV (MW/MVar) at node i.
$P_i^{\text{WT}}, Q_i^{\text{WT}}$ Active/reactive power injections of the WT (MW/MVar) at node i.
$P_i^{\text{L}}, Q_i^{\text{L}}$ Active/reactive loads (MW/MVar) at node i.
$\bar{P}_i^{\text{PV}}, \zeta_i^{\text{PV}}$ Predicted value and forecasting error (MW) of the PV active power at node i.
$\bar{P}_i^{\text{WT}}, \zeta_i^{\text{WT}}$ Predicted value and forecasting error (MW) of the WT active power at node i.
$\bar{P}_i^{\text{L}}, \zeta_i^{\text{L,P}}$ Predicted value and forecasting error (MW) of the active load at node i.
$\bar{Q}_i^{\text{L}}, \zeta_i^{\text{L,Q}}$ Predicted value and forecasting error (MW) of the reactive load at node i.
$\hat{P}_i^{\text{PV}}, \hat{Q}_i^{\text{PV}}$ Actual active/reactive power injections of the PV (MW/MVar) at node i after curtailment.
$\hat{P}_i^{\text{WT}}, \hat{Q}_i^{\text{WT}}$ Actual active/reactive power injections of the WT (MW/MVar) at node i after curtailment.

E. Constants

$P_{m,i}^{\min}, P_{m,i}^{\max}$ Minimum/maximum active power (MW) of the m-th controllable DG at bus i.
$Q_{m,i}^{\min}, Q_{m,i}^{\max}$ Minimum/maximum reactive power (MVar) of the m-th DG at bus i.
$\Delta P_{m,i}^{\max}, \Delta Q_{m,i}^{\max}$ Maximum active/reactive ramping power (MW/MVar) of the m-th DG at bus i.
$P_{s,i}^{\text{d,min}}, P_{s,i}^{\text{d,max}}$ Minimum/maximum discharging power (MW) of the s-th SU at bus i.
$P_{s,i}^{\text{c,min}}, P_{s,i}^{\text{c,max}}$ Minimum/maximum charging power (MW) of the s-th SU at bus i.
$\Delta P_{s,i}^{\text{d,max}}, \Delta P_{s,i}^{\text{c,max}}$ Maximum discharging/charging ramping power (MW) of the s-th SU at bus i.
$SoC_{s,i}^{\min}, SoC_{s,i}^{\max}$ Minimum/maximum state of charge (%) of the s-th SU at bus i.
$E_{s,i}^{\max}$ Rated capacity (MWh) of s-th SU at bus i.
$\Delta T, T$ Time step and prediction horizon.
$\eta_{s,i}$ Self-discharging coefficient of the s-th SU at bus i accounting for internal energy losses.
$\eta_{s,i}^{\text{d}}, \eta_{s,i}^{\text{c}}$ Energy efficiencies during discharging and charging processes of the s-th SU at bus i.
$Q_{c,i}^{\max}, \Delta Q_{c,i}^{\text{step}}$ Maximum reactive power and power step (MVar) of the c-th SSC at bus i.
$\Delta Q_{c,i}^{\max}$ Maximum reactive ramping power (MVar) of the c-th SSC at bus i.
$t_{o,ij}^{\max}$ Maximum tap position of o-th OLTC between buses i and j to regulate secondary voltages.
$\Delta t_{o,ij}^{\max}$ Maximum value of tap change of the o-th OLTC between buses i and j.
k_{ij}^{fix} Standard ratio of the OLTC between buses i and j without OLTC regulations.
$k_{o,ij}^{\min}, k_{o,ij}^{\max}$ Minimum/maximum ratios of the o-th OLTC between buses i and j.
$\Delta k_{o,ij}$ Change step of the relative ratio of o-th OLTC between buses i and j.
$\dot{Y}_m^o, \dot{Y}_T^o$ Shunt and serial admittances of the o-th OLTC.
$\boldsymbol{\mu}_x$ Weighting matrix (\$/pu^2) of voltage deviations.
$\boldsymbol{x}^{\text{ref}}$ Referential voltage magnitudes of 1.0 pu.
$G_{\text{P}}^{\text{cDG}}, G_{\text{Q}}^{\text{cDG}}$ Cost coefficients for active (\$/MWh) and reactive power (\$/MVarh) of controllable DGs.
G^{SSC} Cost coefficient of SSCs (\$/MVarh).
R^{OLTC} Cost coefficient for OLTC actions (\$).
$N_{s,i}^{\min}$ Minimum number of cycles of the s-th SU at bus i when depth of discharge equals one.
$C_{s,i}^{\text{SU}}$ Investment cost (\$) of the s-th SU at bus i.
α, β Cost coefficients for active power (\$/MWh) and reactive power (\$/MVarh).
$\boldsymbol{\mu}_{\text{PV}}, \boldsymbol{\mu}_{\text{WT}}$ Penalty matrices (\$/MWh) for renewable power abandonment of PVs and WTs.
$\boldsymbol{A}, \boldsymbol{A}_{\text{loss}}$ Identity matrices in the state space model and linear approximation of power losses.
$\hat{\boldsymbol{B}}, \hat{\boldsymbol{D}}$ Sensitivity matrices (pu/MW, pu/MVar) indicating variations of voltage magnitudes with respect to control and disturbance variables.
$\boldsymbol{B}_{\text{loss}}, \boldsymbol{D}_{\text{loss}}$ Sensitivity matrices (pu/MW, pu/MVar) indicating variations of power losses with respect to control variables and disturbance variables.

I. Introduction

THE integration of large-scale distributed renewable energy has imposed severe uncertainties on modern distribution network operation [1]–[3]. The economical and reliable control strategies are required to be determined against fluctuating generation outputs and unforeseeable meteorological conditions. Moreover, increasingly complicated end-users aggravate the stochastic characteristic of load profiles. The active distribution network (ADN) is a promising alternative of

traditional passive network management to accommodate cleaner renewable energy and enlarge the integration of distributed generation. Active distribution networks are distribution networks that have systems in place to control a combination of distributed energy resources (generators, loads and storage) [4], [5]. Distributed system operators have the possibility of managing electric flows with the support of distributed energy resources and a flexible network topology. Resorting to advanced control schemes, ADNs improve system flexibility and operational reliability. Therefore, stochastic control of ADNs is needed to account for inherent uncertainties of distributed renewable energy [6] and system loads.

Extensive studies focusing on optimal control and optimization of active distribution networks have been carried out. A centralized voltage constraints management method [7] was proposed to minimize distributed generation curtailment, and a detailed curtailment strategy based on voltage-sensitivity factors was studied in [8]. An adaptive reactive power control scheme [9] in a radial distribution system with large installation of photovoltaic (PV) cells was presented for direct handling of trade-offs between minimizing power losses and satisfying voltage regulations. However, [7]–[9] merely concentrated on static analyses at one snapshot without simulation studies along time-series, of which applicability is insufficient to consider time-variant renewable power generation [10] and system loads, and incorporate temporal dynamics of storage devices.

To tackle this problem, model predictive control (MPC) [11] has drawn great attention recently for the optimal control of ADNs [12]–[14]. The core idea behind MPC is to solve a finite-horizon optimal control problem based on predicted information of system dynamics. This multi-step characteristic of MPC is similar with dynamic optimal power flow [15] and multi-period optimization [16], [17]. Thus, MPC can sufficiently anticipate future events and systematically consider multivariable constraints. Furthermore, MPC realizes an implicit feedback control law with repeated solutions of optimal control problems in a receding horizon manner, which can compensate modeling inaccuracies and measurement noises, and mitigate computational complexities compared with dynamic programming [15]. However, previous works [12]–[14] were usually based on deterministic model predictive control (DMPC). A rolling horizon optimization of active distribution networks based on MPC was proposed in [13] to enhance secure operation and load balance of feeder lines utilizing loop power flow controllers. Reference [14] developed a two-level voltage correction scheme to regulate various distributed generators (DGs). The power generation of intermittent renewable sources was modeled as predicted time series in previous studies. Although the implicit closed-loop nature of MPC offers a certain degree of robustness, its deterministic formulation is inherently inadequate to model volatile power of intermittent renewable sources due to the ignorance of probabilistic information [18] and leads to potentially infeasible control actions.

This paper proposes a stochastic receding horizon control (SRHC) method based on modified stochastic model predictive control (SMPC) to tackle fluctuating renewable energy and loads. Inspired by relevant standards and grid codes [19], [20], the voltage limitations are reformulated as chance constraints to involve the probabilistic reliability index of voltage qualification rate, which is defined as a statistical percentage that the voltage deviation is within an acceptable range. The control strategies of various controllable means, including regulations of distributed generators, switchable shunt capacitors (SSCs), storage units (SUs) and on load tap changing transformers (OLTCs), are obtained through solving a chance-constrained multi-period optimization problem. SMPC has recently emerged to systematically incorporate stochastic information of real-world systems, which has been used in storage management [21] and microgrids [22]. However, to authors' best knowledge, there are rarely studies aiming at comprehensive stochastic control of ADNs based on SMPC. Moreover, traditional SMPC uses Jacobian-based sensitivities to predict system dynamics, which have heavy computational burden in application. To overcome this deficiency, the simplified Z-bus sensitivity for active distribution network is developed for efficient approximation of system nonlinearity, and is combined with the sequential linear programming (SLP) [23] to iteratively derive the linear state space model (SSM) for compensation of cumulative modeling errors. Resorting to the simplified Z-bus approach and sequential linear programming, the overall performance of the proposed SRHC method with respect to modeling accuracy and computing efficiency is significantly improved, which consequently contributes to more reliable and precise decision of control strategies. In particular, the Z-bus method [24] utilizes information of nodal power injections for rapid update of sensitivities, which improves computational efficiency with high accuracy compared with the Jacobian-based method used in [8], [12]–[14].

Compared with traditional "soft" relaxation of voltage constraints [13], chance constraints can achieve trade-offs between minimization of control costs and requirement of voltage regulations. Some works in optimal power flow [25]–[27] and unit commitment [28] also use chance constraints to account for impacts of uncertainty on system regulation. A affine-disturbance feedback policy is utilized here to enhance close-loop voltage regulation and analytically convert intractable chance constraints into second-order cone constraints. The final problem can be solved effectively via mixed-integer second-order cone programming.

This paper provides contributions in the following aspects:

1) A novel stochastic receding horizon control method based on modified SMPC framework is developed by integrating the simplified Z-bus sensitivity, sequential linear programming and disturbance feedback control. Various distributed controllable resources are jointly optimized to facilitate economical and reliable operation of ADNs against severe uncertainties of renewable energy and loads.

2) The simplified Z-bus sensitivity for active distribution networks is developed for computationally efficient estimation of system nonlinearity while guaranteeing modeling accuracy. The simplified Z-bus approach is then combined with sequential linear programming in the proposed SRHC method to iteratively derive the linear state space model for compensation of cumulative modeling errors.

3) The disturbance feedback control policy is employed in the proposed SRHC method to counteract disturbance effects and guarantee the close-loop control performance. The voltage limitations are reformulated as chance constraints to indicate the probabilistic reliability index of voltage qualification rate and achieve trade-offs between cost reduction and voltage regulation. The affine-disturbance parameterization is utilized to render the stochastic chance-constrained problem computationally solvable via mixed-integer second-order cone programming.

4) The superiority and validity of the proposed SRHC method in terms of control performance, voltage violation, cost reduction and scalability are validated through systematic case studies of 33-bus and 123-bus test systems compared with other schemes, namely DMPC, stochastic model predictive control with hard constraints (SMPC-HC) and the open-loop control (OLC).

5) Comprehensive multi-objective formulation is developed to indicate the performance of voltage regulation, control costs and penalties of renewable energy curtailment, which can achieve coordination of controllable resources.

The remainder of this paper are organized as follows: Section II proposes the mathematical model of active distribution systems for the optimization purpose. In Section III, the problem formulation of the stochastic receding horizon control strategy is given in details with the objective function, hard constraints, chance constraints, the derivation of sensitivity matrices and the illustration of the proposed SRHC strategy. Comprehensive case studies based on 33-bus and 123-bus test systems are presented in Section IV. Finally, conclusions and findings are drawn in Section V.

II. Modeling of Active Distribution Network

A. Distributed Renewable Energy and Load

To indicate uncertainties associated with renewable energy and loads, in this paper power generations of PVs, wind turbines (WTs), and loads, are represented by times series of predicted values combined with forecasting errors [29], [30]. Forecasting errors are assumed to follow the normal distribution with zero mean, which has been widely recognized to identify the presence of forecasting errors in previous studies [27], [31]. Active power of PVs, WTs, and system demands are formulated as

$$P_i^{\mathrm{PV}}(t)=\bar{P}_i^{\mathrm{PV}}(t)+\zeta_i^{\mathrm{PV}}(t),\boldsymbol{\zeta}_i^{\mathrm{PV}}\in N\left(0,\boldsymbol{\sigma}_i^{\mathrm{PV}}\right),i\in\mathcal{I}^{\mathrm{PV}},t\in\mathcal{T} \quad (1)$$

$$P_i^{\mathrm{WT}}(t)=\bar{P}_i^{\mathrm{WT}}(t)+\zeta_i^{\mathrm{WT}}(t),\boldsymbol{\zeta}_i^{\mathrm{WT}}\in N\left(0,\boldsymbol{\sigma}_i^{\mathrm{WT}}\right),i\in\mathcal{I}^{\mathrm{WT}},t\in\mathcal{T} \quad (2)$$

$$\begin{cases} P_i^{\mathrm{L}}(t)=\bar{P}_i^{\mathrm{L}}(t)+\zeta_i^{\mathrm{L,P}}(t),\boldsymbol{\zeta}_i^{\mathrm{L,P}}\in N\left(0,\boldsymbol{\sigma}_i^{\mathrm{L,P}}\right) \\ Q_i^{\mathrm{L}}(t)=\bar{Q}_i^{\mathrm{L}}(t)+\zeta_i^{\mathrm{L,Q}}(t),\boldsymbol{\zeta}_i^{\mathrm{L,Q}}\in N\left(0,\boldsymbol{\sigma}_i^{\mathrm{L,Q}}\right) \\ i\in\mathcal{I}^{\mathrm{L}},t\in\mathcal{T} \end{cases} \quad (3)$$

Power injections of PVs and WTs are counted at coupling points so that power losses of inverters are already included. With the deployment of curtailment mechanism, the renewable energy generation can be regulated into a lower level. The actual power injections absorbed by the network after curtailment are evidently less than the available outputs, namely

$$\begin{cases} \hat{P}_i^{\mathrm{PV}}(t)\le P_i^{\mathrm{PV}}(t),\hat{Q}_i^{\mathrm{PV}}(t)\le Q_i^{\mathrm{PV}}(t),i\in\mathcal{I}^{\mathrm{PV}},t\in\mathcal{T} \\ \hat{P}_i^{\mathrm{WT}}(t)\le P_i^{\mathrm{WT}}(t),\hat{Q}_i^{\mathrm{WT}}(t)\le Q_i^{\mathrm{WT}}(t),i\in\mathcal{I}^{\mathrm{WT}},t\in\mathcal{T} \end{cases} \quad (4)$$

B. Controllable Distributed Generator

The controllable DGs are synchronous machines including coal-based generators or microturbines. The active and reactive power outputs can be regulated via proper control strategies. The generation limits and ramping limits are formulated as

$$\begin{cases} P_{m,i}^{\min}\le P_i^{\mathrm{cDG}}(t)\le P_{m,i}^{\max},|\Delta P_i^{\mathrm{cDG}}(t)|\le\Delta P_{m,i}^{\max} \\ Q_{m,i}^{\min}\le Q_i^{\mathrm{cDG}}(t)\le Q_{m,i}^{\max},|\Delta Q_i^{\mathrm{cDG}}(t)|\le\Delta Q_{m,i}^{\max} \\ i\in\mathcal{I}^{\mathrm{cDG}},m\in\mathcal{M},t\in\mathcal{T} \end{cases} \quad (5)$$

C. Distributed Storage Unit

The distributed SUs can provide ADNs with operational flexibility for relieving intermittency of renewable energy due to their fast-response capability. A crucial feature of storage units is the time coupling characteristic related with state of charge (%), indicated by

$$\begin{aligned} SoC_i^{\mathrm{SU}}(t+1)=\ & \eta_{s,i}SoC_i^{\mathrm{SU}}(t) \\ & +\frac{\Delta T}{E_{s,i}^{\max}}\left(\eta_{s,i}^{\mathrm{c}}P_i^{\mathrm{c,SU}}(t)-\frac{1}{\eta_{s,i}^{\mathrm{d}}}P_i^{\mathrm{d,SU}}(t)\right) \end{aligned} \quad (6)$$

where $\eta_{s,i}^{\mathrm{d}}$ means the proportion of power feed-in to the distribution network divided by actual discharging power. Similarly, $\eta_{s,i}^{\mathrm{c}}$ indicates the ratio of charging power divided by power injection from the distribution network. Limits on charging (discharging) power, ramping rate and the state of charge of storage units, and non-simultaneous constraints on charging and discharging processes are indicated by

$$\begin{cases} v_i^{\mathrm{d,SU}}(t)P_{s,i}^{\mathrm{d,min}}\le P_i^{\mathrm{d,SU}}(t)\le v_i^{\mathrm{d,SU}}(t)P_{s,i}^{\mathrm{d,max}} \\ v_i^{\mathrm{c,SU}}(t)P_{s,i}^{\mathrm{c,min}}\le P_i^{\mathrm{c,SU}}(t)\le v_i^{\mathrm{c,SU}}(t)P_{s,i}^{\mathrm{c,max}} \\ |\Delta P_i^{\mathrm{d,SU}}(t)|\le\Delta P_{s,i}^{\mathrm{d,max}},|\Delta P_i^{\mathrm{c,SU}}(t)|\le\Delta P_{s,i}^{\mathrm{c,max}} \\ SoC_{s,i}^{\min}\le SoC_i^{\mathrm{SU}}(t)\le SoC_{s,i}^{\max} \\ v_i^{\mathrm{d,SU}}(t)+v_i^{\mathrm{c,SU}}(t)\le 1,i\in\mathcal{I}^{\mathrm{SU}},s\in\mathcal{S},t\in\mathcal{T} \end{cases} \quad (7)$$

D. Switchable Shunt Capacitor

The SSCs consist of a number of capacitor banks that can be connected to, or disconnected from, the network by controllable switches. Switchable shunt capacitors can act as reactive power sources typically installed in ADNs for Volt/VAR control. In this paper, SSCs are modeled as reactive power sources [13], [32] with capacity and ramping constraints, shown in (8). The discrete nature of the capacitor bank is also considered by including the integer number $N_i^{\mathrm{C}}(t)$ in reactive power

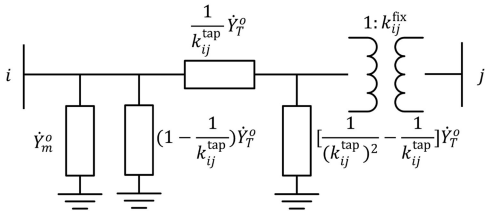

Fig. 1. Equivalent circuit of the OLTC.

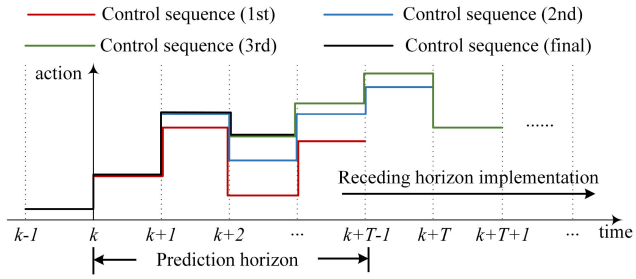

Fig. 2. Illustration of multi-step receding horizon control procedure.

compensation, given as

$$\begin{cases} 0 \le Q_i^{\text{C}}(t) \le Q_{c,i}^{\max}, |\Delta Q_i^{\text{C}}(t)| \le \Delta Q_{c,i}^{\max} \\ Q_i^{\text{C}}(t) = N_i^{\text{C}}(t) \Delta Q_{c,i}^{\text{step}} \\ i \in \mathcal{I}^{\text{C}}, c \in \mathcal{C}, t \in \mathcal{T} \end{cases} \tag{8}$$

E. On Load Tap Changing Transformer

The on load tap changing transformer is usually equipped with an automatic voltage regulator to control secondary bus voltage through actions of on load tap changer. Assume that the o-th OLTC is placed between bus i and j and equivalent circuit is shown in Fig. 1. Limits on tap positions, transformer ratios and the relationship between tap positions and transformer ratios are denoted as

$$\begin{cases} 1 \le t_{ij}^{\text{OLTC}}(t) \le t_{o,ij}^{\max}, |\Delta t_{ij}^{\text{OLTC}}(t)| \le \Delta t_{o,ij}^{\max} \\ k_{o,ij}^{\min} \le k_{ij}(t) = k_{ij}^{\text{fix}} k_{ij}^{\text{tap}}(t) \le k_{o,ij}^{\max} \\ k_{ij}^{\text{tap}}(t) = (t_{ij}^{\text{OLTC}}(t) - 1)\Delta k_{o,ij} + \dfrac{k_{o,ij}^{\min}}{k_{ij}^{\text{fix}}} \\ \Delta k_{o,ij} = \dfrac{k_{o,ij}^{\max} - k_{o,ij}^{\min}}{k_{ij}^{\text{fix}}(t_{o,ij}^{\max} - 1)}, i,j \in \mathcal{I}^{\text{OLTC}}, o \in \mathcal{O}, t \in \mathcal{T} \end{cases} \tag{9}$$

Tap regulations can change the bus admittance matrix, leading to an unsolvable problem. Therefore, the OLTC model is modified with fictitious current injections [33], given as,

$$\begin{cases} \Delta \dot{I}_i = -\dot{U}_i(\dot{Y}_m^o + \dot{Y}_T^o) + \dot{U}_j \dot{Y}_T^o \dfrac{1}{k_{ij}^{\text{tap}}} \\ \Delta \dot{I}_j = \dot{U}_i \dot{Y}_T^o \dfrac{1}{k_{ij}^{\text{tap}}} - \dot{U}_j \dot{Y}_T^o \dfrac{1}{(k_{ij}^{\text{tap}})^2} \end{cases} \tag{10}$$

and detailed derivation of the equivalent fictitious current injections can be found in Appendix A.

III. Problem Formulation of Stochastic Receding Horizon Control Strategy

A. Objective Function

The proposed SRHC approach is typically a multi-step, receding horizon method. The control actions of various controllable resources are obtained through solving a T-horizon chance-constrained optimization problem with minimization of the objective function while satisfying all system constraints. The prediction horizon T is a core concept in SMPC which indicates the time span of finite-horizon optimization. For instance, if the time granularity is 15 minutes, then 4-horizon optimization means an hour-ahead control. At each time instant, control solutions are acquired through solving a 4-horizon optimization problem. Only the current (or the first) time-step control move is implemented and at the next sampling time, the optimization problem is reformulated and solved with new measurements and updated state space models over a shifted horizon. As illustrated in Fig. 2, the whole control procedure is carried out in a receding horizon manner. The prediction horizon keeps being shifted forward with repeated solutions of optimal control problems. The final control sequence (denoted as black line) is the combination of first-time-slot actions of the control sequences obtained from each implementation.

The proposed SRHC strategy of ADN minimizes voltage deviations from referential setpoints and control costs of various controllable resources. The degradation cost of SU is taken into account to enhance its service life. The cost penalizing renewable generation curtailment is also considered to promote the low-carbon electricity. In this paper, state vector $\boldsymbol{x}(t)$ denotes voltage magnitudes of all buses measured in pu and control vector $\boldsymbol{u}(t)$ represents power setpoints of controllabe DGs, SSCs, SUs, and tap positions of OLTCs respectively. The objective is formulated in form of conditional expectation with initial state $\boldsymbol{x}(t|t)$, expressed as

$$\begin{aligned} \min \boldsymbol{J} = \mathbb{E}_{\boldsymbol{x}(t|t)} \big[& \boldsymbol{F}(\boldsymbol{x}) + \boldsymbol{Y}(\boldsymbol{u}) + \boldsymbol{W}(\boldsymbol{E}^{\text{SU}}) \\ & + \boldsymbol{V}(\boldsymbol{P}^{\text{CP}}, \boldsymbol{Q}^{\text{CP}}) + \boldsymbol{D}(\boldsymbol{P}^{\text{PV}}, \hat{\boldsymbol{P}}^{\text{PV}}, \boldsymbol{P}^{\text{WT}}, \hat{\boldsymbol{P}}^{\text{WT}}) \big] \end{aligned} \tag{11}$$

where $\boldsymbol{F}(\cdot)$, $\boldsymbol{Y}(\cdot)$, $\boldsymbol{W}(\cdot)$, $\boldsymbol{V}(\cdot)$, and $\boldsymbol{D}(\cdot)$ refer to the cost of voltage deviations, control costs of various controllable resources, the degradation cost of SUs, the power exchange tariff to the utility, and the cost penalizing renewable generation abandonment respectively. The cost of voltage deviations $\boldsymbol{F}(\cdot)$ is defined as

$$\begin{aligned} \boldsymbol{F}(\boldsymbol{x}) = \sum_{k=0}^{T-1} \Delta T \big[& (\boldsymbol{x}(t+k+1|t) - \boldsymbol{x}^{\text{ref}})^{\intercal} \boldsymbol{\mu}_x \\ & (\boldsymbol{x}(t+k+1|t) - \boldsymbol{x}^{\text{ref}}) \big] \end{aligned} \tag{12}$$

where $\boldsymbol{\mu}_x$ is the weighting matrix penalizing the voltage fluctuation. Control costs $\boldsymbol{Y}(\cdot)$ is formulated as

$$\boldsymbol{Y}(\boldsymbol{u}) = \sum_{k=0}^{T-1} \Delta T \left[\boldsymbol{u}(t+k)^{\intercal} \boldsymbol{R}\boldsymbol{u}(t+k) + \boldsymbol{G}\boldsymbol{u}(t+k)\right] \quad (13)$$

where control costs of controllable DGs and SSCs are proportional to their active or reactive power outputs, while cost for OLTC regulations is in a quadratic form of change step of tap position. The degradation cost of SUs $\boldsymbol{W}(\cdot)$ is expressed as

$$\boldsymbol{W}(\boldsymbol{E}^{\mathrm{SU}}) = \sum_{k=0}^{T-1} \sum_{i \in \mathcal{I}^{\mathrm{SU}}} \frac{C_{s,i}^{\mathrm{SU}}}{N_i^{\mathrm{SU}}(t+k)} \quad (14)$$

where $N_i^{\mathrm{SU}}(t)$ denotes the number of remaining cycles of the SU at bus i, given by

$$N_i^{\mathrm{SU}}(t) = \frac{N_{s,i}^{\min}}{D_i^{\mathrm{SU}}(t)} = \frac{N_{s,i}^{\min}}{1 - SoC_i^{\mathrm{SU}}(t)} \quad (15)$$

where $D_i^{\mathrm{SU}}(t)$ refers to the depth of discharge. The power exchange tariff to the main grid $\boldsymbol{V}(\cdot)$ is defined as

$$\boldsymbol{V}(\boldsymbol{P}^{\mathrm{CP}}, \boldsymbol{Q}^{\mathrm{CP}}) = \sum_{k=0}^{T-1} \sum_{i \in \mathcal{I}^{\mathrm{CP}}} \Delta T \left[\alpha P_i^{\mathrm{CP}}(t+k) + \beta Q_i^{\mathrm{CP}}(t+k)\right] \quad (16)$$

where α and β are the prices of active and reactive power. The curtailment cost of renewable energy $\boldsymbol{D}(\cdot)$ is formulated as

$$\boldsymbol{D}(\boldsymbol{P}^{\mathrm{PV}}, \hat{\boldsymbol{P}}^{\mathrm{PV}}, \boldsymbol{P}^{\mathrm{WT}}, \hat{\boldsymbol{P}}^{\mathrm{WT}}) = \sum_{k=0}^{T-1} \Delta T \Big[\boldsymbol{\mu}_{\mathrm{PV}} \big(\boldsymbol{P}^{\mathrm{PV}}(t+k) - \hat{\boldsymbol{P}}^{\mathrm{PV}}(t+k)\big) + \boldsymbol{\mu}_{\mathrm{WT}} \big(\boldsymbol{P}^{\mathrm{WT}}(t+k) - \hat{\boldsymbol{P}}^{\mathrm{WT}}(t+k)\big)\Big] \quad (17)$$

where $\boldsymbol{\mu}_{\mathrm{PV}}$ and $\boldsymbol{\mu}_{\mathrm{WT}}$ are coefficient matrices penalizing energy curtailment of PVs and WTs respectively.

B. Hard Constraints

In this paper, all constraints of the proposed SRHC method can be classified into two groups: hard and chance constraints, with different physical implications in system modeling. Hard constraints contain the state space models, control limits, state of charge limits, power balances, etc., which cannot be violated to avoid system malfunction or infeasible control actions. In contrast, chance constraints are required to be satisfied with at least a priori specified probability level. A small violation of the chance constraints is allowable to achieve trade-offs between cost reduction and voltage regulations. This is the case for voltage constraints. The hard constraints of the optimal control problem of ADNs are listed as

$$\text{s.t. } \boldsymbol{x}(t+k+1|t) = \boldsymbol{A}\boldsymbol{x}(t+k|t) + \hat{\boldsymbol{B}}\boldsymbol{\Delta u}(t+k) + \hat{\boldsymbol{D}}\boldsymbol{\Delta d}(t+k) \quad (18)$$

$$\boldsymbol{\Delta u}(t+k) = \boldsymbol{u}(t+k+1) - \boldsymbol{u}(t+k) \quad (19)$$

$$\boldsymbol{u}^{\min} \le \boldsymbol{u}(t+k) \le \boldsymbol{u}^{\max} \quad (20)$$

$$\boldsymbol{0} \le \boldsymbol{\Delta u}(t+k) \le \boldsymbol{\Delta u}^{\max} \quad (21)$$

$$\boldsymbol{SoC}^{\mathrm{SU}}(t+k+1) = \boldsymbol{\eta}\boldsymbol{SoC}^{\mathrm{SU}}(t+k) + \frac{\Delta T}{\boldsymbol{E}^{\max}}(\boldsymbol{\eta}^{\mathrm{c}}\boldsymbol{P}^{\mathrm{c,SU}} - \boldsymbol{\eta}^{\mathrm{d}}\boldsymbol{P}^{\mathrm{d,SU}}) \quad (22)$$

$$\boldsymbol{SoC}^{\min} \le \boldsymbol{SoC}^{\mathrm{SU}}(t+k) \le \boldsymbol{SoC}^{\max} \quad (23)$$

$$\sum_{i \in \mathcal{I}^{\mathrm{cDG}}} P_i^{\mathrm{cDG}}(t+k) + \sum_{i \in \mathcal{I}^{\mathrm{PV}}} \hat{P}_i^{\mathrm{PV}}(t+k) + \sum_{i \in \mathcal{I}^{\mathrm{WT}}} \hat{P}_i^{\mathrm{WT}}(t+k) + \sum_{i \in \mathcal{I}^{\mathrm{SU}}} P_i^{\mathrm{d,SU}}(t+k) + P_i^{\mathrm{CP}}(t+k) - \sum_{i \in \mathcal{I}^{\mathrm{SU}}} P_i^{\mathrm{c,SU}}(t+k) - \sum_{i \in \mathcal{I}^{\mathrm{L}}} P_i^{\mathrm{L}}(t+k) = P_{\mathrm{loss}}(t+k) \quad (24)$$

$$\sum_{i \in \mathcal{I}^{\mathrm{cDG}}} Q_i^{\mathrm{cDG}}(t+k) + \sum_{i \in \mathcal{I}^{\mathrm{PV}}} \hat{Q}_i^{\mathrm{PV}}(t+k) + \sum_{i \in \mathcal{I}^{\mathrm{WT}}} \hat{Q}_i^{\mathrm{WT}}(t+k) + \sum_{i \in \mathcal{I}^{\mathrm{C}}} Q_i^{\mathrm{C}}(t+k) + Q_i^{\mathrm{CP}}(t+k) - \sum_{i \in \mathcal{I}^{\mathrm{L}}} Q_i^{\mathrm{L}}(t+k) = Q_{\mathrm{loss}}(t+k) \quad (25)$$

$$\boldsymbol{L}(t+k+1) = \boldsymbol{A}_{\mathrm{loss}}\boldsymbol{L}(t+k) + \boldsymbol{B}_{\mathrm{loss}}\boldsymbol{\Delta u}(t+k) + \boldsymbol{D}_{\mathrm{loss}}\boldsymbol{\Delta d}(t+k) \quad (26)$$

$$\boldsymbol{u}(t|t) = \boldsymbol{u}(t) \quad (27)$$

$$\boldsymbol{x}(t|t) = \boldsymbol{x}(t), \forall k \in \mathcal{T} \quad (28)$$

where equality constraint (18) refers to the state space model indicating voltage evolution; constraints (19)–(21) denote control limits obtained through combing (5), (7)–(9); constraints (22) and (23) indicate the state of charge limit of storage units; active and reactive power balances with losses are represented by (24)–(25); the linear approximation of losses is expressed as (26), which indicates variations of active and reactive power losses with respect to control and disturbance variables; constraints (27) and (28) are the initial conditions of control and state variables.

In (18), the linear SSM is utilized here to incorporate voltage deviations with respect to control actions and external disturbances. State vector $\boldsymbol{x}(t)$ denotes voltage magnitudes of all buses measured in pu. The variation of control variables, i.e., $\boldsymbol{\Delta u}(t)$, defines adjustments of active and reactive power of controllable DGs, active power of SUs, reactive power of SSCs, and tap regulations of OLTCs. $\boldsymbol{\Delta d}$ represents exogenous disturbances of PVs, WTs and loads, which can be captured by their forecasting errors. $\boldsymbol{A}$ is the identity matrix in the state space model (18). $\hat{\boldsymbol{B}}$ and $\hat{\boldsymbol{D}}$ are sensitivity matrices with units of pu/MW and pu/MVar, indicating variations of voltage magnitudes with respect to control variables and disturbance variables.

These sensitivity matrices are obtained using the simplified Z-bus method given in the next section. In (26), the symbol $\boldsymbol{L}$ refers to $\boldsymbol{L}(t) = [P_{\text{loss}}(t), Q_{\text{loss}}(t)]^{\intercal}$; $\boldsymbol{A}_{\text{loss}}$ represents the identity matrix in the linear approximation of power losses; $\boldsymbol{B}_{\text{loss}}$ and $\boldsymbol{D}_{\text{loss}}$ express how much power losses change after small changes of control and disturbance variables.

C. Derivation of Sensitivity Matrix

Jacobian-based sensitivity analysis is widely used in model predictive control [12]–[14]. However, it encounters computational burdens because of the full Newton-Raphson power flow calculation. If voltages are assumed to be constant instead (namely $\dot{U} = 1\angle 0^{\circ}$), the fixed sensitivities may be highly inaccurate [24]. These features make Jacobian-based sensitivities inadequate for SLP implementation as receding horizon manner requires frequent renewal of sensitivity matrices with desired accuracies.

To achieve a trade-off between computational efficiency and precision, a simplified Z-bus method for active distribution networks is developed in this paper for system linearization with high computational efficiency and desirable accuracy. The Z-bus sensitivity coefficients are explicit functions of voltages $\dot{U}_i$ and power injections $\widetilde{S}_i$ [24] while the Jacobian-based sensitivities are merely functions of voltage magnitudes and angles. Assuming that the voltages are constant, the simplified Z-bus sensitivities are more precise than constant Jacobian sensitivities due to the partially modified information of nodal power injections. The simplified Z-bus sensitivities improve computational efficiency with acceptable approximation errors without reliance on power flow solutions, which can be utilized in on-line estimation. In this paper, there are two categories of sensitivity matrices, namely voltage magnitude sensitivity matrix and power loss sensitivity matrix, corresponding to the sensitivity matrices in the state space model (18) and linear approximation of power losses (26) respectively. For simplicity, only the derivative of voltage magnitude of bus i with respect to active power at node k are illustrated by

$$\frac{\partial U_i}{\partial P_k} = \frac{1}{U_i}\Re\left(\bar{U}_i \frac{\partial \dot{U}_i}{\partial P_k}\right), i \in \mathcal{I}^{\text{IN}} \tag{29}$$

$$\frac{\partial \dot{U}_i}{\partial P_k} = \sum_{j \in \mathcal{I}^{\text{IN}}} \frac{-\dot{Z}_{ij}\bar{S}_j}{\bar{U}_j^2}\frac{\partial \bar{U}_j}{\partial P_k} + \frac{\dot{Z}_{ik}\bar{U}_k}{\bar{U}_k^2}, k \in \mathcal{I}^{\text{IN}} \tag{30}$$

where U_i and $\dot{U}_i$ denote the voltage magnitude and complex voltage of bus i respectively; $\dot{Z}_{ij}$ is the complex bus impedance between buses i and j; $\Re$ is the operator calculating the real component of a complex numbers; $\bar{U}_j$ and $\bar{S}_j$ here refer to the conjugate variables of $\dot{U}_j$ and $\widetilde{S}_j$ respectively. Other sensitivities of voltage magnitudes and power losses can be obtained similarly and are given in Appendix B.

D. Chance Constraints

In some grid codes [19], the voltage qualification rate is defined as a probabilistic index indicating statistical proportion of voltage deviation within an acceptable range, such as 95% for urban power grids in China [20], because it is not practical to absolutely maintain the voltage within an interval. Thus, voltage magnitudes are reformulated as chance constraints instead of traditional soft relaxations [13]. Additionally, by introducing a small level of constraint violation, control costs can be reduced to avoid expensive control actions. Chance constraints on voltage magnitudes are given as

$$\Pr\{U_i^{\min} \le U_i \le U_i^{\max}\} \ge 1 - \epsilon, i \in \mathcal{I}^{\text{IN}} \tag{31}$$

Chance constraints are generally non-convex and intractable, and this paper leverages affine-disturbance parameterization [34] to analytically convert chance constraints into second order cone constraints. Besides, by introducing the affine-disturbance feedback policy, the control actions are linearly mapped with the disturbance variables to achieve better close-loop performance of the stochastic control strategy. With the affine-disturbance feedback law, control input $\boldsymbol{\Delta u}(t)$ is parameterized as an affine function of the disturbance variables for decision of corrective actions, given by

$$\boldsymbol{\Delta u}(t) = \boldsymbol{h}(t) + \sum_{j=0}^{t-1} \boldsymbol{M}_{t,j}\boldsymbol{\Delta d}(j) \tag{32}$$

where $\boldsymbol{h}(t) \in \mathbb{R}^U$ and $\boldsymbol{M}_{t,j} \in \mathbb{R}^{U\times R}$, U and R are dimensions of control and disturbance vectors. The control input (32) is further transformed into block matrix form by augmenting vectors and matrices to include variables along the prediction horizon, expressed as

$$\boldsymbol{\pi} = \widetilde{\boldsymbol{M}} \times \boldsymbol{\omega} + \widetilde{\boldsymbol{h}} \tag{33}$$

where $\boldsymbol{\pi} \in \mathbb{R}^{T\cdot U}$, $\widetilde{\boldsymbol{M}} \in \mathbb{R}^{T\cdot U\times T\cdot R}$, $\boldsymbol{\omega} \in \mathbb{R}^{T\cdot R}$, $\widetilde{\boldsymbol{h}} \in \mathbb{R}^{T\cdot U}$, $\boldsymbol{\pi}$, $\boldsymbol{\omega}$, $\widetilde{\boldsymbol{h}}$ and $\widetilde{\boldsymbol{M}}$ are extensions of $\boldsymbol{\Delta u}$, $\boldsymbol{\Delta d}$, $\boldsymbol{h}$ and $\boldsymbol{M}$ respectively. The affine function transforms decision variables from $\boldsymbol{\pi}$ to $\widetilde{\boldsymbol{M}}$ and $\widetilde{\boldsymbol{h}}$. After affine-disturbance parameterization, the state space model is reformulated as

$$\boldsymbol{\Phi} = \widetilde{\boldsymbol{A}}\boldsymbol{x}(0) + \boldsymbol{H}\widetilde{\boldsymbol{h}} + \boldsymbol{L}\widetilde{\boldsymbol{M}}\boldsymbol{\omega} + \boldsymbol{E}\boldsymbol{\omega} \tag{34}$$

where $\boldsymbol{\Phi} \in \mathbb{R}^{T\cdot N}$, $\widetilde{\boldsymbol{A}} \in \mathbb{R}^{T\cdot N\times N}$, $\boldsymbol{H} \in \mathbb{R}^{T\cdot N\times T\cdot U}$, $\boldsymbol{L} \in \mathbb{R}^{T\cdot N\times T\cdot U}$, $\boldsymbol{E} \in \mathbb{R}^{T\cdot N\times T\cdot R}$, $\boldsymbol{\Phi}$ is a column vector containing nodal voltage magnitudes from $t = 1$ to $t = T$. The detailed structures of these matrices can be found in Appendix C. The joint chance constraint (31) on voltage magnitudes can be separated into two individual chance constraints with corresponding upper and lower bounds [35], [36]. Chance constraints of the proposed SRHC method are given as

$$\Pr\{\boldsymbol{G}_i\boldsymbol{\Phi} \le U_i^{\max}\} \ge 1 - \frac{\epsilon}{2} \tag{35}$$

$$\Pr\{\boldsymbol{G}_i\boldsymbol{\Phi} \ge U_i^{\min}\} \ge 1 - \frac{\epsilon}{2} \tag{36}$$

where $\forall i \in \mathbb{Z}_1^{T\cdot N}$, $\boldsymbol{G}_i \in \mathbb{R}^{1\times T\cdot N}$, and the elements in row vector $\boldsymbol{G}_i$ are all zeros except that the i-th element is assigned to 1. The chance constraints are pointwise-in-time. In other words, the voltage of any bus $i \in \mathcal{I}^{\text{IN}}$ at each time instant $t \in \mathcal{T}$ should satisfy the preceding chance constraints. Note that the

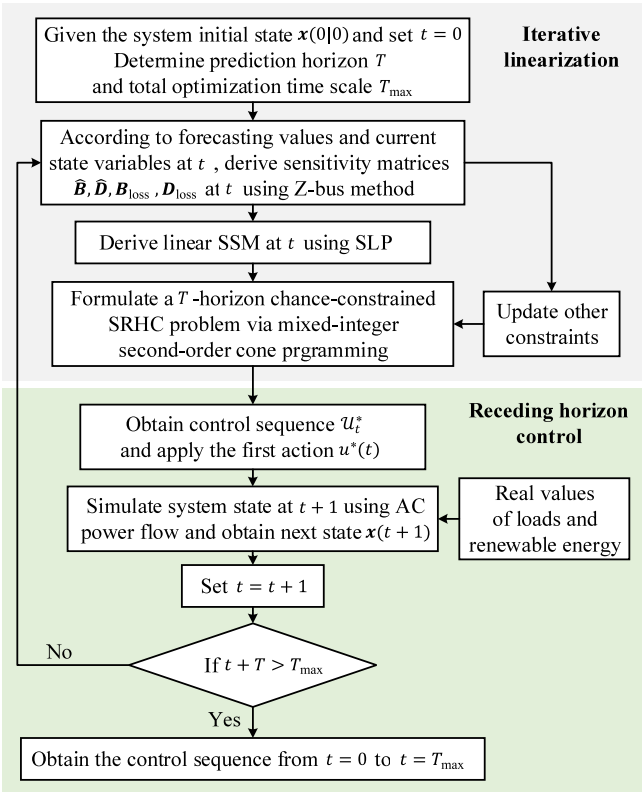

Fig. 3. Flowchart of the stochastic receding horizon control strategy.

chance constraints (35) and (36) are bi-affine in the decision variables $\widetilde{\boldsymbol{M}}$ and $\widetilde{\boldsymbol{h}}$ and the disturbances $\boldsymbol{\omega}$. Following the assumption of normal distributions of random variables, the individual chance constraints can be analytically formulated as deterministic second-order cone constraints, expressed as

$$\varphi^{-1}\left(1-\frac{\epsilon}{2}\right)||\boldsymbol{G}_i(\boldsymbol{L}\widetilde{\boldsymbol{M}}+\boldsymbol{E})\boldsymbol{\sigma}||_2 \leq U_i^{\max}-\boldsymbol{G}_i(\widetilde{\boldsymbol{A}}\boldsymbol{x}(0)+\boldsymbol{H}\widetilde{\boldsymbol{h}}) \quad (37)$$

$$\varphi^{-1}\left(\frac{\epsilon}{2}\right)||\boldsymbol{G}_i(\boldsymbol{L}\widetilde{\boldsymbol{M}}+\boldsymbol{E})\boldsymbol{\sigma}||_2 \geq U_i^{\min}-\boldsymbol{G}_i(\widetilde{\boldsymbol{A}}\boldsymbol{x}(0)+\boldsymbol{H}\widetilde{\boldsymbol{h}}) \quad (38)$$

where φ is the standard Gaussian cumulative distribution function, and $\boldsymbol{\sigma}$ is the covariance matrix of disturbance $\boldsymbol{\omega}$.

E. Stochastic Receding Horizon Control Strategy

A detailed flow chart demonstrating the proposed SRHC strategy is shown in Fig. 3, composed of iterative linearization and receding horizon control. Here the total control time scale $T_{\max}$ refers to the whole temporal span of receding horizon control. The system states are initialized at $t = 0$. At each time instant t, sensitivity matrices in the SSM are updated based on current measured states and control inputs, and the forecasting values of renewable energy and system loads. A T-horizon chance-constrained SRHC problem is formulated based on forecasting values of renewable energy and loads from t to $t + T - 1$, and current measured states at t, containing objective (11), hard constraints (18)–(28), and chance constraints (37), (38). The affine-disturbance parameterization is utilized to transform chance constraints into second-order cone constraints. Then the optimal T-step control sequence $\mathcal{U}^* \triangleq \{\boldsymbol{u}^*(t), \ldots, \boldsymbol{u}^*(t+T-1)\}$ is obtained by solving a mixed-integer second-order cone programming problem. Only the first input $\boldsymbol{u}^*(t)$ is actually applied to the system. After implementing control actions, system states at $t+1$ are simulated using AC power flow and real values of loads and renewable energy. At next instant $t+1$, the problem is reformulated with full state measurements combined with $\pm 1\%$ white noise[12]. The linear SSM is updated according to system states and forecasting values with shifted operational conditions based on simplified Z-bus sensitivities and sequential linear programming. This stochastic control strategy is carried out in a receding horizon manner with iterative linearization, until the control actions of the whole time scale (from $t = 0$ to $t = T_{\max}$) are obtained. By modifying the traditional SMPC with iterative linearizaion in each implementation of receding horizon control, the proposed SRHC strategy can improve estimation accuracy with affordable computational complexity, and thereby contribute to more precise determination of control strategies. Besides, the simplified Z-bus sensitivity provides an efficient method for on-line linearization of AC power flow equations.

It is worth noting that control actions are obtained through solving mixed-integer second-order cone programming problems. Nonlinearity introduced by AC power flow has been eliminated by iterative linearization based on simplified Z-bus sensitivities. The second-order cone programming is proved to be convex and can be solved effectively [37], [38]. Thus, convergence of the proposed method can be guaranteed with manageable computational complexity.

In summary, the schematic diagram of the proposed SRHC method is illustrated in Fig. 4. The core part of the stochastic receding horizon control method is the problem formulation based on simplified Z-bus sensitivities and sequential linear programming. The state space models capturing system dynamics are iteratively updated in the receding horizon manner. Control actions are obtained through solving a mixed-integer second-order cone programming problem, which are applied in the distribution system to check state evolutions.

IV. Simulation Results

A. System Configuration

The modified 33-bus, 12.66 kV distribution system [39] on a per phase basis is utilized to verify the proposed SRHC approach. The single-line diagram is shown in Fig. 5. Bus 1 is the slack bus connecting to the main grid. The OLTC is placed between Buses 2 and 3. The tap changer has 9 discrete positions with a ratio step of 5%. The regulating range of secondary voltage is $\pm 20\%$. The test system is modified to include renewable generation and various controllable devices. There are 2 controllable DGs with the capacity of 2×1.0 MW, namely DG_1 and DG_2 respectively, and 2 SSCs with the capacity of 2×0.8 MVar, namely SSC_1 and SSC_2 respectively. Adjustment step of reactive power compensation is 0.05 MVar for each SSC. The PV_1

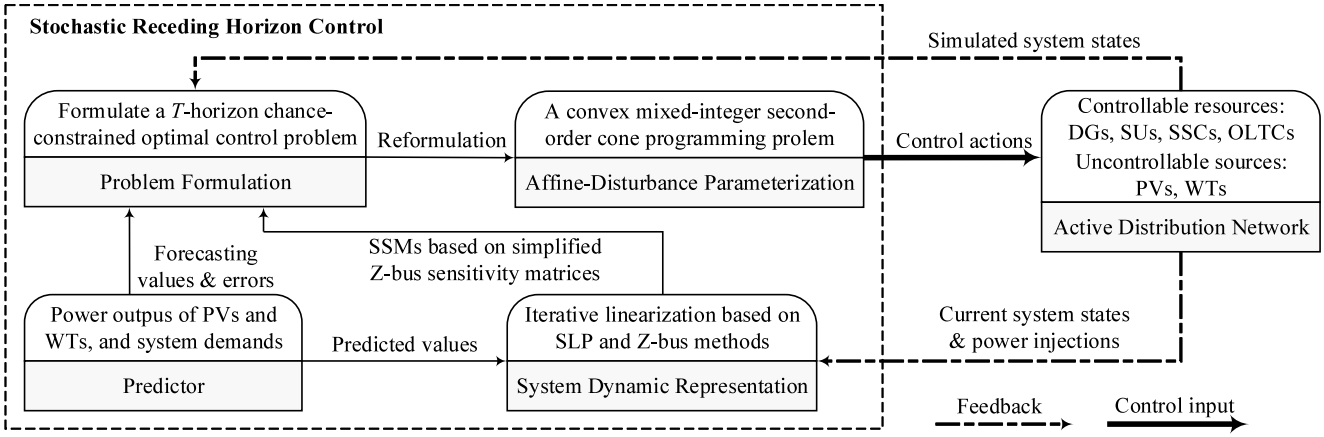

Fig. 4. Schematic diagram of the proposed SRHC method.

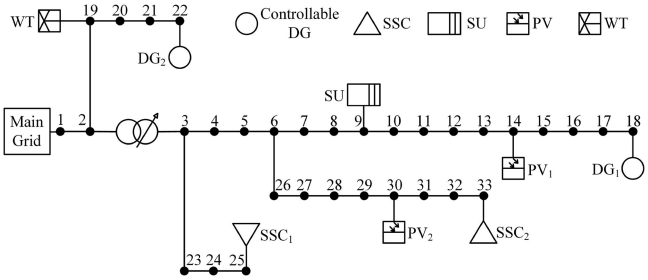

Fig. 5. Network of the modified 33-bus distribution system.

TABLE I
OBJECTIVE PARAMETERS

Item	Value	Item	Value	Item	Value
μ_x	10000 \$/pu^2	$G_{\mathrm{P}}^{\mathrm{cDG}}$	17 \$/MWh	$G_{\mathrm{Q}}^{\mathrm{cDG}}$	15 \$/MVarh
G^{SSC}	10 \$/MVarh	R^{OLTC}	30 \$	$C_{s,i}^{\mathrm{SU}}$	1.5×10^6 \$
$N_{s,i}^{\min}$	20000	α	36 \$/MWh	β	30 \$/MVarh
μ_{PV}	50 \$/MWh	μ_{WT}	50 \$/MWh		

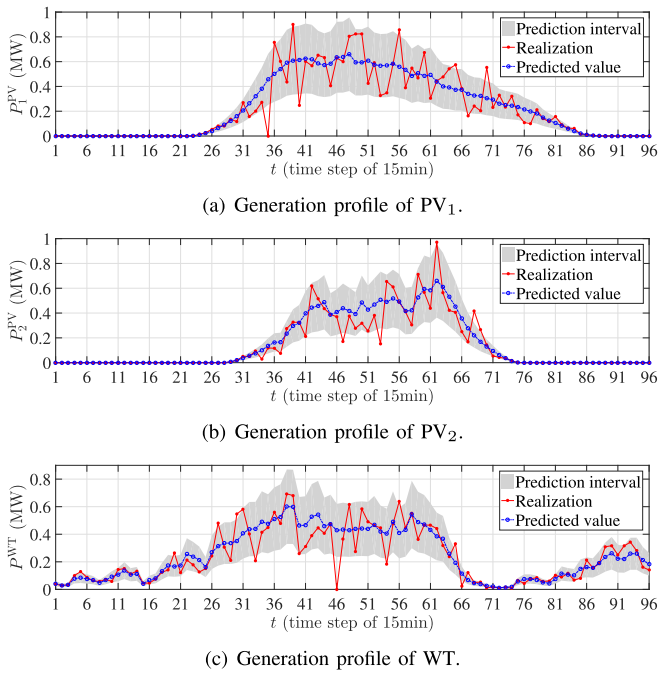

(a) Generation profile of PV_1.

(b) Generation profile of PV_2.

(c) Generation profile of WT.

Fig. 6. Output profiles of renewable energy.

and PV_2 are located at Buses 14 and 30 with the capacity of $2 \times 1.0\ \mathrm{MW_p}$. The WT and SU are situated at Buses 19 and 9 with the capacity of $1.0\ \mathrm{MW_p}$ and 1 MWh respectively. The total time scale $T_{\max}$ is 24 hours with granularity of $T = 15$ minutes. The predefined violation level is fixed at $\epsilon = 0.025$, i.e., a 2.5% probability of voltage violation is allowed in optimization. To ensure voltage quality, the weighting parameter of voltage deviation carries a bigger weight than the others. Other parameters in the objective function are shown in Table I.

The peak load is approximately 4.70 MW. The standard deviation of normal distribution capturing forecasting errors is assumed to be $\sigma = 10\%$ of the predicted values. Fig. 6 shows predicted active power of PV_1, PV_2, and WT in blue lines, as well as prediction intervals and actual output realizations (red lines). The prediction intervals quantify forecasting errors with a confidence level of 95%. Note that the renewable generations show a certain degree of fluctuation so that the effectiveness and robustness of the proposed SRHC method can be illustrated more clearly under this typical scenario.

B. Accuracy of Sensitivity and SSM

1) Sensitivity: To illustrate the sensitivity accuracy, Jacobian-based sensitivities are employed as benchmarks to evaluate accuracy of the proposed SRHC method using the simplified Z-bus sensitivity. Let $\boldsymbol{A}_{\mathrm{J}}$, $\boldsymbol{A}_{\mathrm{Z}}$, and $\boldsymbol{A}_{\mathrm{Zsim}}$ denote the Jacobian-based, Z-bus, and simplified Z-bus sensitivity matrices with fixed voltages ($\dot{U} = 1\angle 0°$), respectively. The relative errors of Z-bus and simplified Z-bus sensitivity matrix compared

TABLE II
COMPUTATIONAL TIME AND RELATIVE ERRORS

Method	Time(s)	$\delta(\%)$
Jacobian	0.7442	0.00
Z-bus	0.7633	6.33×10^{-19}
Simplified Z-bus	0.0180	4.45×10^{-2}

with the Jacobian-based sensitivity are calculated by

$$\delta_1 = \frac{\sum_i \sum_j (A_{\mathrm{Z}}(i,j) - A_{\mathrm{J}}(i,j))^2}{\sum_i \sum_j (A_{\mathrm{J}}(i,j))^2}$$
$$\delta_2 = \frac{\sum_i \sum_j (A_{\mathrm{Zsim}}(i,j) - A_{\mathrm{J}}(i,j))^2}{\sum_i \sum_j (A_{\mathrm{J}}(i,j))^2} \quad (39)$$

Table II details the computational time and relative errors δ of these three methods with the same initial conditions. These results are obtained based on parameters of the modified 33-bus distribution system by MATLAB using an i7-7700 @3.60 GHz, 16GB RAM workstation. The Z-bus sensitivity matrix is almost identical to the Jacobian-based sensitivity matrix. The relative error of simplified Z-bus sensitivities is also acceptable with a small error less than 1%, and the computational time can be tremendously reduced compared with Jacobian and Z-bus sensitivities due to the ellipsis of AC power flow.

Without loss of generality, Bus 10 is selected to verify the accuracy of sensitivities with the change of nodal power injections. The active power of DG_1 at Bus 18 increases gradually from 0.0 MW to 1.0 MW while the other power injections remain unchanged. Fig. 7(a) illustrates the performance of simplified Z-bus sensitivity methodology. The Z-bus sensitivities are exactly the same with the Jacobian-based sensitivities because they both use full AC power flow solutions. The simplified Z-bus method also produced reasonably good approximation based on the constant voltages because the slope of simplified Z-bus sensitivities is similar with Jacobian-based slope. In contrast, the sensitivities calculated by constant Jacobian matrix correspond to horizontal dashed lines, which have significant errors under large deviations.

2) SSM: The voltage magnitude solutions of the proposed SRHC method are compared with AC power flow solutions. Changes of $\Delta P_{18} = 0.6$ MW and $\Delta Q_{25} = 1.2$ MVar are hypothetically imposed on Buses 18 and 25 respectively, indicating the state transition from the origin condition after changes of power injections. Fig. 7(b) illustrates voltage profiles of the whole system. The green crosses denote original voltage magnitudes without changes. This plot confirms that the proposed SRHC method based on the linear SSM is accurate enough for linear estimation because the SSM results (red circles) overlaps real voltages (blue dots) approximately.

C. Verification of Prediction Horizon and SLP

1) Prediction Horizon: One of the key advantages of the proposed SRHC method is the capability of considering future information in current time-slot optimization. Two indicators, namely minimal objective value (MOV, \$), and steady-state

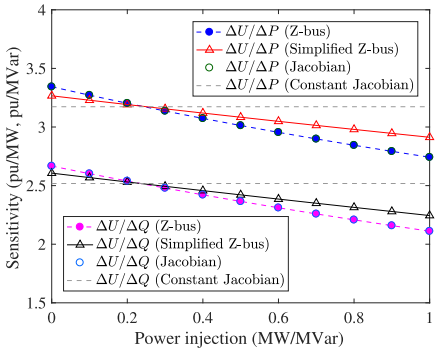

(a) $\Delta U_{10}/\Delta P_{18}$ and $\Delta U_{10}/\Delta Q_{18}$.

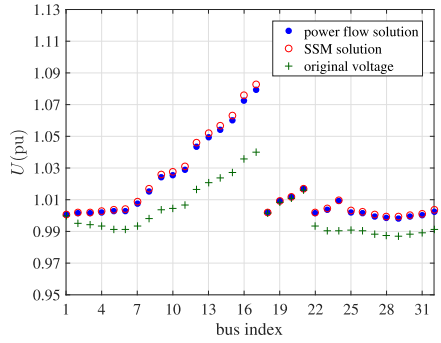

(b) Voltage profiles.

Fig. 7. Accuracy of sensitivities and SSM.

TABLE III
VALIDITY OF THE PROPOSED SRHC METHOD USING SLP

T^1	MOV (\$)			SSVD (pu^2)		
	Fixed	SLP	$\gamma(\%)$	Fixed	SLP	$\gamma(\%)$
2	2169.3	2131.4	1.75	1.4180	1.3751	3.03
4	1762.5	1682.1	4.56	0.9848	0.9098	7.62
6	1633.6	1627.6	0.37	0.8950	0.8659	3.25
8	1564.5	1546.4	1.16	0.8542	0.8068	5.55
10	1419.1	1395.8	1.64	0.7850	0.7294	7.08
12	1410.8	1384.3	1.88	0.7792	0.7217	7.38

[1]The time step is 15 minutes.

voltage deviation (SSVD, pu^2), defined in (40), are applied to demonstrate the optimality and control performance with different prediction horizons.

$$\mathrm{SSVD} = \frac{1}{N} \sum_{i=1}^{N} \sum_{t=1}^{T_c} (U_i(t) - U_{\mathrm{ref}})^2 \quad (40)$$

The curves indicating MOV and SSVD with varying prediction horizon are shown in Fig. 8. When the prediction horizon is extended from 3 to 21, corresponding to 45 minutes- and 315 minutes-ahead stochastic control, the results show exponential improvements on both MOV and SSVD. These plots confirm that strategy optimality and control performance of the proposed SRHC method are enhanced through extending the prediction horizon.

2) SLP: The effectiveness of the proposed SRHC method using SLP compared with a fixed programming method is demonstrated in Table III. Here the fixed method means that the linear

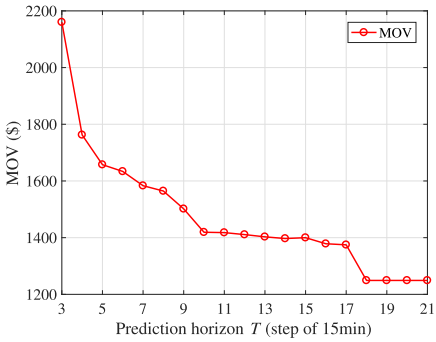

(a) Minimal objective value.

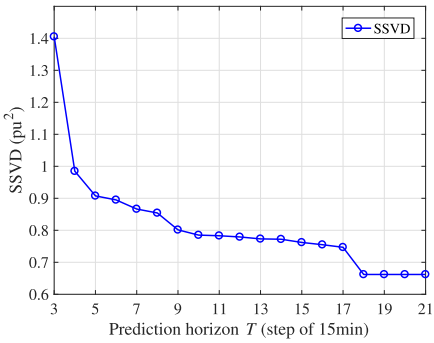

(b) Steady-state voltage deviation.

Fig. 8. Improvements on MOV and SSVD with extending prediction horizon.

SSM is constant over the whole control period of 24 hours without iterative renewals over shifted horizons. Multiple prediction horizons are selected, ranging from $T = 2$ to $T = 12$. After implementing SLP, the overall performance is improved on both MOV and SSVD. The relative improvement is shown as γ. The decrements of SSVD exceed 5% in most cases without increasing optimal minimization value.

D. Simulation Results Using the SRHC Method

With the time interval of 15 minutes, a 10-horizon stochastic receding horizon control of ADNs is demonstrated in Fig. 9 along a whole day. The performed voltage corrections of 5 typical buses are presented in Fig. 9(d). The voltage fluctuation of U_{18} is the most severe, followed by U_{10} and U_{33}, due to the fact that these buses are close to PVs. Fig. 9(g) indicates final statistical distribution of system voltages. This histogram is plotted using voltage magnitudes of all buses from $t = 1$ to $t = 96$. The voltages are confined within desired limit of [0.96, 1.04] in most cases, except for occasional violation ($U > 1.04$). The violation rate τ is 0.94%, which satisfies the predefined violation level of 2.5%.

Fig. 9(a) details corresponding evolution of SU. Due to the intensive power fluctuation induced by intermittent sources and demands, SU serves as a fast-response balancing resource and regulates its charging (discharging) power persistently to handle with the voltage deviations. SoC^{SU} reaches 100% repeatedly to absorb abundant power. The active and reactive power adjustments of controllable DGs and SSCs are shown in Fig. 9(b) and Fig. 9(c) respectively. These devices change their generation

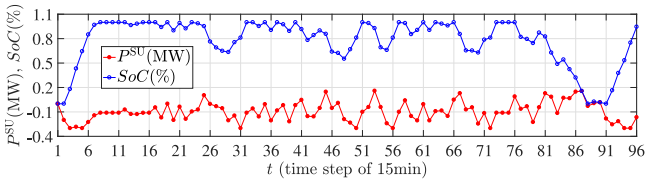

(a) Control results of the SU.

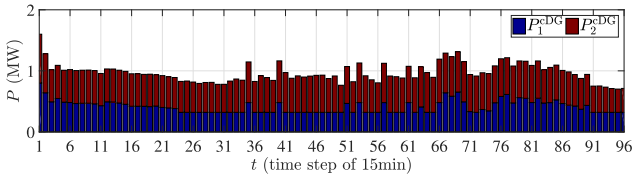

(b) Active power adjustments of controllable DGs.

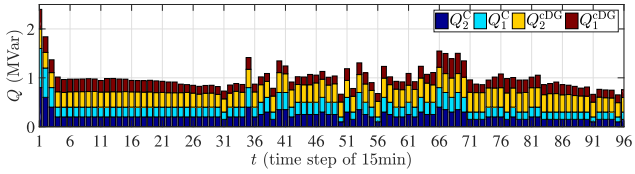

(c) Reactive power adjustments of controllable DGs and SSCs.

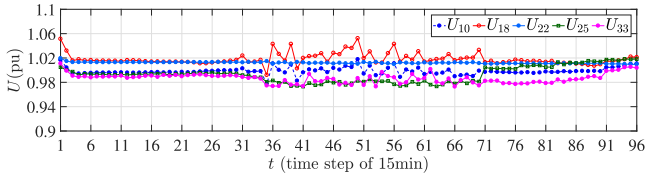

(d) Voltage magnitude profiles.

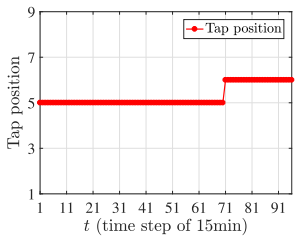

(e) Control results of the OLTC.

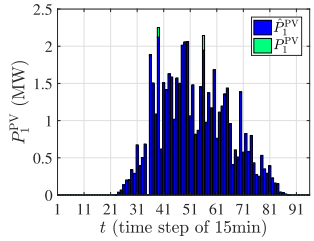

(f) Active power curtailment of PV_1.

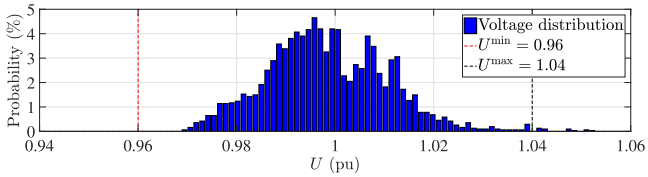

(g) Voltage distribution.

Fig. 9. Stochastic control results under fluctuating generations and demands.

scheduling in diurnal time more frequently than other periods to tackle increasingly volatile power outputs of PV_1 and PV_2. Controllable DGs play a critical role in maintaining active power balance while SSCs are mainly in charge of reactive power regulation relieving voltage fluctuation. Because of the high cost of OLTC actions, the tap position stays idle unless the voltage magnitudes exceed the acceptable region globally, shown in Fig. 9(e).

The detailed curtailment strategies of PV_1 are shown in Fig. 9(f). The blue bars demonstrate the real power outputs

$\hat{P}_i^{\mathrm{PV}}(t)$ accommodated by system and green bars correspond to abandoned power. PV_1 is located at Bus 14 and thereby has severe impacts on the voltage fluctuation of U_{18}. The voltage peaks of U_{18} at $t = 36, 39, 56$ in Fig. 9(d) are eliminated by power curtailment of PV_1 and the curtailment strategy is proved to be effective. There is no curtailment of PV_2 because U_{33} remains in normal region. In brief, the proposed SRHC method can effectively maintain system voltage within the desired interval. Various control resources ranging from controllable DGs and SSCs to renewable energy curtailment and SUs are operated in coordination to provide balancing power and mitigate voltage fluctuations. Chance constraints are also proved to take effect in guaranteeing voltage deviations under a pre-defined probability level.

E. Effectiveness Analysis of the SRHC Method

The aim of this section is to validate effectiveness and superiority of the proposed approach. For this purpose, the simulation studies are carried out through comparison of following methods: 1) deterministic model predictive control utilizing a deterministic formulation without consideration of forecasting errors and enforcing soft voltage constraints for feasibility; 2) stochastic model predictive control with hard constraints, where chance constraints on voltage magnitudes are replaced by hard constraints; 3) stochastic receding horizon control with chance constraints, namely the proposed SRHC approach; 4) perfect bound control (PBC) given perfect knowledge of future information. The PBC is selected as a theoretical benchmark to investigate practical potential of SRHC. Fig. 10 depicts comparison results of these four methods in terms of violation rate τ, additional control cost measure in percentage compared with PBC, and control performance represented by SSVD. Here the control cost ($) refers to MOV without the voltage deviation penalty cost. It can be found that PBC shows no violation as well as the smallest control cost as expected. SRHC clearly has significantly control cost, smaller amount of voltage violations, and better control performance compared with DMPC. This assessment result indicates that the proposed SRHC method can efficiently anticipate future uncertainty information and significantly exploit improvement potentials to derive economic and reliable control strategies. By incorporating chance constraints on voltage magnitudes, SRHC has a slightly higher violation rate (0.94%) than SMPC-HC (0%), whereas the control cost is reduced significantly due to the prevention of expensive control actions by allowing a small prescribed violation level ($\epsilon = 2.5\%$).

To investigate impacts of uncertainty levels on control results, Table IV reports comparison results of four methods with different standard deviations of forecasting errors, ranging from $\sigma = 5\%$ to $\sigma = 15\%$. Three scenarios with different levels of uncertainties are utilized here to demonstrate the performance of the proposed SRHC method. It is worth noting that the additional cost is measured in percentage corresponding to PBC cost benchmark under the same level of forecasting errors. With the increasing levels of forecasting errors, the cost benchmark of PBC consistently grows to tackle volatile power sources and demands. SRHC shows significant improvements on cost reduction and voltage regulation in comparison with DMPC. When standard deviation is 15% of predicted values, DMPC can cause 14.91% additional cost and a voltage violation rate of 6.68%, while SRHC is confirmed to effectively restrict voltage violation at a level of 1.51% with additional cost of 4.13%. Although SMPC-HC has 100% constraint satisfaction, more expense on control actions will be paid, such as more than 3.0% extra cost compared with SRHC when $\sigma = 10\%$, and even no feasible solutions if the forecasting errors exceed 15%. Table IV also indicates that SRHC shows more potential in terms of cost reduction and violation restriction compared with DMPC with

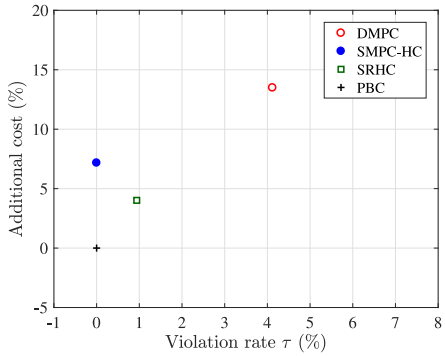

(a) Additional cost and violation rate.

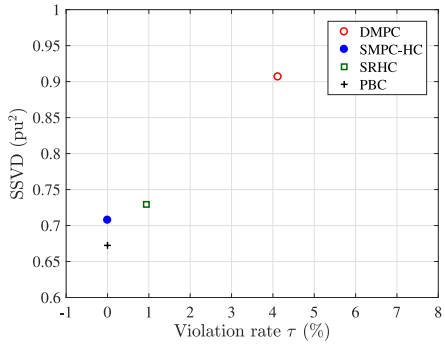

(b) SSVD and violation rate.

Fig. 10. Performance comparison of four methods.

TABLE IV
PERFORMANCE COMPARISON OF FOUR METHODS WITH DIFFERENT UNCERTAINTY LEVELS

	Uncertainty level[1]	5%	10%	15%
DMPC	Additional cost (%)[2]	12.27	13.49	14.91
	Violation rate τ (%)	2.90	4.12	6.68
SMPC-HC	Additional cost (%)	5.52	7.17	–[3]
	Violation rate τ (%)	0.00	0.00	–
SRHC	Additional cost (%)	3.77	4.02	4.13
	Violation rate τ (%)	0.80	0.94	1.51
PBC	Cost benchmark ($)	905.54	928.80	988.06
	Violation rate τ (%)	0.00	0.00	0.00

[1] The uncertainty level is indicated by the standard deviation of forecasting error.
[2] Addition cost is measured in percentage compared with PBC cost under the same level of uncertainty.
[3] "–" means infeasible.

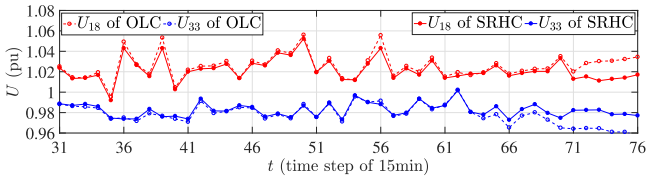

Fig. 11. Voltage profiles using the SRHC and OLC.

TABLE V
CONTROL STRATEGY COMPARISON OF THE SRHC AND OLC

Method	MOV ($)	SSVD (pu^2)	τ (%)
SRHC	1395.8	0.7294	0.94
OLC	1561.8	0.9669	1.79

the ascending levels of forecasting errors. The violation rate has been diminished from 2.90% to 0.80% when $\sigma = 5\%$, while this gap is enlarged to more than 5% when $\sigma = 15\%$, from 6.68% to 1.51%. It thus can be concluded that more control costs can be saved with more satisfactory voltage regulation by replacing DMPC with the proposed SRHC method as uncertainties grow larger.

Furthermore, the proposed SRHC method is compared with the open-loop control strategy to validate its superiority. The OLC is optimized only once for the whole time span $T_{\max}$ without iterative update of SSMs and repeated problem reformulations. The receding horizon control manner is also removed from the OLC, as well as the disturbance feedback policy. Fig. 11 shows the voltage profiles of U_{18} and U_{33} using the SRHC and OLC. The OLC leads to a large deviation of voltage magnitudes. The voltage peak of U_{18} reaches nearly 1.06 at $t = 56$. There are also larger variations of U_{18} and U_{33} from $t = 71$ to $t = 76$. In contrast, SRHC ensures more stable performance of voltage regulations. Numerical results of these two control methods with multiple evaluation criteria are reported in Table V. The SRHC performs better than the OLC in terms of the voltage violation, objective function value and control performance.

F. Trade-Offs of Chance Constraints

The incorporation of chance constraints on voltages can achieve trade-offs between cost reduction and voltage satisfaction compared with traditional hard constraints. By assuming higher probability level of constraint violation, one can naturally obtain lower control cost. Fig. 12(a) indicates voltage profile of U_{18} with hard constraints ($\epsilon = 0\%$), chance constraints of $\epsilon = 2.5\%$ and chance constraints of $\epsilon = 10.0\%$. Under the limitations of hard constraints, U_{18} is always under 1.04 p.u., leading to conservative behaviors, expensive control actions and extra renewable power curtailment. In contrast, U_{18} with chance constraints is less conservative due to the violations of voltage upper bound and the violation degree can be adaptively regulated with different predefined level.

Fig. 12(b) depicts a tuning curve describing trade-offs between control costs ($) and predefined violation level (ϵ, %).

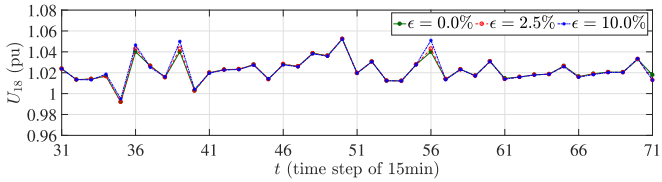

(a) Voltage profile of U_{18} with different chance constraints.

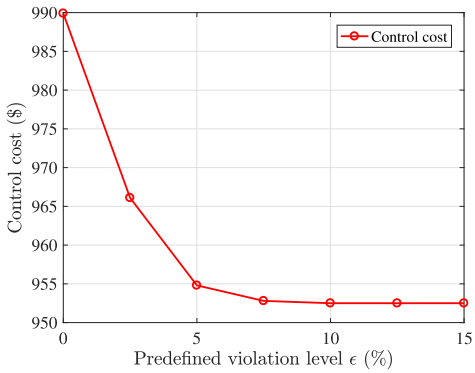

(b) Trade-offs between control costs and violation rate.

Fig. 12. Trade-offs of chance constraints.

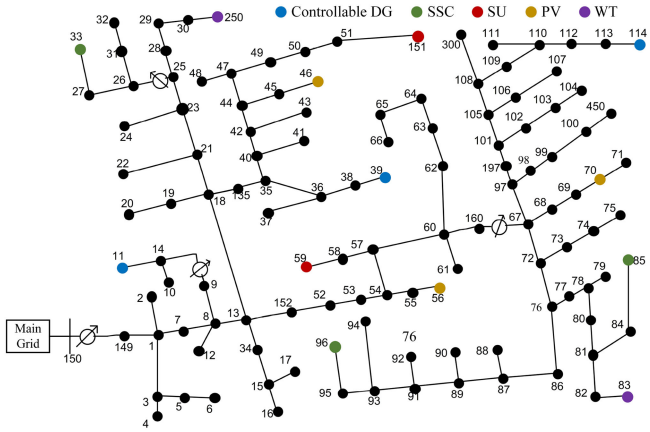

Fig. 13. Network of the modified 123-bus distribution system.

The trade-offs between control costs and voltage restrictions can be achieved by means of allowing a predefined level of constraint violation. Evidently, the proposed SRHC method is proved to have the capability of reducing control costs significantly by decreasing the satisfaction rate of voltage constraints with only a small level.

G. Tests on the Large System

A modified IEEE 123-bus distribution system [40] is used to test the effectiveness and scalability of the proposed SRHC method on larger systems. The radial topology is shown in Fig. 13 associated with locations of various distributed energy resources. Only phase A is selected with the balanced configuration. In total, there are 3 controllable DGs, 3 SSCs, 2 SUs and 4 OLTCs. The test feeders are also modified to include 3 PVs and 2 WTs. The total loads are approximately 8.06 MW and 3.65 MVar.

TABLE VI
VALIDATION OF SCALABILITY

Scale	Method	Cost ($)	SSVD (pu^2)	τ (%)
33-bus	SRHC	966.1	0.7294	0.94
	DMPC	1054.1	0.9068	4.12
123-bus	SRHC	1634.9	0.9350	1.16
	DMPC	1826.8	1.2669	3.95

TABLE VII
COMPARISON OF COMPUTATIONAL TIME

Scale	Method	AT (s)	AOT(s)	AUT (s)
33-bus	SRHC-Jacobian	3.62	1.2429	0.7356
	SRHC	2.21	1.2429	0.0205
123-bus	SRHC-Jacobian	26.23	12.0334	6.2693
	SRHC	16.86	12.0334	0.0424

The comparison between the proposed SRHC method and the DMPC method is given in Table VI when they are implemented in 33-bus and 123-bus test systems. The SRHC performs better than the DMPC in terms of control costs and voltage regulation. In the 123-bus test feeders, the control cost can be reduced by 10.50% from 1826.8$ to 1634.9$. The violation rate of voltage constraints can also be improved using the proposed approach. In a word, the proposed stochastic receding horizon control strategy shows good scalability and is proved to effectively enhance system voltage quality and reduce control costs in larger systems.

To verify the computational efficiency, a detailed report of computational time is illustrated in Table VII with the comparison between the proposed SRHC method and the stochastic control strategy using Jacobian-based sensitivities (SRHC-Jacobian). The main difference between SRHC and SRHC-Jacobian is that SRHC-Jacobian uses Jacobian-based sensitivities for iterative linearization while the proposed SRHC uses simplified Z-bus sensitivities. Three criteria are given for evaluation, including the average time of implementing control actions at one time instant (AT), the average optimization time (AOT) and the average SSM update time (AUT). Generally AT is composed of AOT, AUT, and other time used for problem formulation and assignment in each implementation. The Jacobian-based SSM update requires full solutions of AC power flow. Thus, the AUT of SRHC-Jacobian is much higher than that of SRHC. This is particularly important in larger systems, where the computational burden of updating SSMs rises up dramatically from 0.0424 to 6.2693 seconds for the 123-bus system. As a consequence, the AT can be reduced by nearly 50% if the Jacobian sensitivity is replaced by the simplified Z-bus one. According to the receding horizon manner of the control scheme, optimization problems are solved repeatedly to obtain the control sequence of the whole time scale $T_{\max}$. The total time is calculated by accumulating the computing times of nearly $T_{\max}$ times of implementations and the absolute improvement of the total computing time is more significant in the larger system. Therefore, the proposed SRHC method based on the simplified Z-bus sensitivity can boost computational efficiency significantly and shows good scalability in applications of larger systems.

V. CONCLUSION

In this paper, a stochastic receding horizon control method based on modified SMPC framework is developed for ADNs considering multiple uncertainties of renewable energy and loads. SMPC is modified by incorporating the simplified Z-bus sensitivity, sequential linear programming and disturbance feedback control. The simplified Z-bus method for active distribution networks is developed and combined with SLP for iterative linearization of nonlinear system dynamics with high computational efficiency and desirable accuracy. The voltage limits are reformulated as chance constraints to indicate the probabilistic index of voltage qualification rate and attain trade-offs between cost reduction and constraint satisfaction. The affine-disturbance feedback policy is utilized to enhance close-loop control performance and achieve analytical transformation of intractable chance constraints. The proposed SRHC strategy is carried out in the receding horizon manner. The control strategies of controllable DGs, SSCs, SUs and OLTCs are jointly optimized through solving chance-constrained multi-horizon optimal control problems. Multi-objective formulations are derived to indicate the control performance and coordinated operational costs of these controllable resources. Comprehensive studies based on 33-bus and 123-bus distribution systems are carried out to demonstrate the effectiveness and scalability of the proposed SRHC method.

The proposed SRHC approach can compensate linear approximation inaccuracy without loss of computational efficiency to derive reliable control strategies. Various control resources are jointly coordinated to provide balancing power and guarantee voltage deviations within the desired interval under a priori probability level against uncertainties of renewable energy and load profiles. Control costs and constraint violation are reduced compared with DMPC and open-loop control strategies. Multiple scenarios are utilized to test the method performance with different uncertainty levels of forecasting errors. In conclusion, the proposed SRHC method systematically incorporates the stochastic information of uncertainties and provides an attractive solution for practical control of ADNs.

APPENDIX

A. Derivation of Equivalent Current Injections of the OLTC

The nodal voltage equations of nodes i and j without on load tap changing transformer are given as

$$\begin{bmatrix} \dot{I}_i \\ \dot{I}_j \end{bmatrix} = \begin{bmatrix} \dot{Y}_{ii} & \dot{Y}_{ij} \\ \dot{Y}_{ji} & \dot{Y}_{jj} \end{bmatrix} \times \begin{bmatrix} \dot{U}_i \\ \dot{U}_j \end{bmatrix} \tag{41}$$

where $\dot{Y}_{ii}, \dot{Y}_{ij}, \dot{Y}_{ji}, \dot{Y}_{jj}$ are the elements in the bus admittance matrix. After the insertion of o-th transformer in the branch between nodes i and j, as shown in Fig 1, the expression in (41)

becomes

$$\begin{bmatrix} \dot{I}_i \\ \dot{I}_j \end{bmatrix} = \begin{bmatrix} \dot{Y}_{ii} + \dot{Y}_m^o + \dot{Y}_T^o & \dot{Y}_{ij} - \dot{Y}_T^o \frac{1}{k_{ij}^{\text{tap}}} \\ \dot{Y}_{ji} - \dot{Y}_T^o \frac{1}{k_{ij}^{\text{tap}}} & \dot{Y}_{jj} + \dot{Y}_T^o \frac{1}{(k_{ij}^{\text{tap}})^2} \end{bmatrix} \times \begin{bmatrix} \dot{U}_i \\ \dot{U}_j \end{bmatrix} \quad (42)$$

where $\dot{Y}_m^o$ and $\dot{Y}_T^o$ are the equivalent shunt admittance and the equivalent serial admittance of o-th OLTC. The adjustments of transformer taps are known to result in changes in the bus admittance matrix. Therefore, we modify the model of on load tap changing transformer by incorporation of fictitious current injections [33]. The effect of tap position is reflected by equivalent fictitious current injections $[\Delta\dot{I}_i, \Delta\dot{I}_j]^\intercal$. Thus Equation (42) can be transformed as

$$\begin{bmatrix} \dot{I}_i \\ \dot{I}_j \end{bmatrix} + \begin{bmatrix} \Delta\dot{I}_i \\ \Delta\dot{I}_j \end{bmatrix} = \begin{bmatrix} \dot{Y}_{ii} & \dot{Y}_{ij} \\ \dot{Y}_{ji} & \dot{Y}_{jj} \end{bmatrix} \times \begin{bmatrix} \dot{U}_i \\ \dot{U}_j \end{bmatrix} \quad (43)$$

and fictitious current injections can be derived as

$$\begin{cases} \Delta\dot{I}_i = -\dot{U}_i(\dot{Y}_m^o + \dot{Y}_T^o) + \dot{U}_j \dot{Y}_T^o \dfrac{1}{k_{ij}^{\text{tap}}} \\ \Delta\dot{I}_j = \dot{U}_i \dot{Y}_T^o \dfrac{1}{k_{ij}^{\text{tap}}} - \dot{U}_j \dot{Y}_T^o \dfrac{1}{(k_{ij}^{\text{tap}})^2} \end{cases} \quad (44)$$

B. Sensitivity

The voltage sensitivity of bus i with respect to reactive power at bus k is given by (45) and (46).

$$\frac{\partial U_i}{\partial Q_k} = \frac{1}{U_i} \Re\left(\bar{U}_i \frac{\partial \dot{U}_i}{\partial Q_k} \right), i \in \mathcal{I}^{\text{IN}} \quad (45)$$

$$\frac{\partial \dot{U}_i}{\partial Q_k} = \sum_{j \in \mathcal{I}^{\text{IN}}} \frac{-\dot{Z}_{ij}\bar{S}_j}{\bar{U}_j^2} \frac{\partial \bar{U}_j}{\partial Q_k} - \mathrm{j} \frac{\dot{Z}_{ik}\bar{U}_k}{\bar{U}_k^2}, k \in \mathcal{I}^{\text{IN}} \quad (46)$$

Similarly, the sensitivity of the voltage magnitude with respect to the tap position can be calculated via combining (47) and (48).

$$\frac{\partial U_k}{\partial t_{ij}^{\text{OLTC}}} = \frac{1}{U_k} \Re\left(\bar{U}_k \frac{\partial \dot{U}_k}{\partial t_{ij}^{\text{OLTC}}} \right) \quad (47)$$

$$\begin{aligned} \frac{\partial \dot{U}_k}{\partial t_{ij}^{\text{OLTC}}} = & \left(\dot{Z}_{kj} \dot{Y}_T^o \frac{1}{k_{ij}^{\text{tap}}} - \dot{Z}_{ki} \dot{Y}_m^o - \dot{Z}_{ki} \dot{Y}_T^o \right) \frac{\partial \dot{U}_i}{\partial t_{ij}^{\text{OLTC}}} \\ & + \left(\dot{Z}_{ki} \dot{Y}_T^o \frac{1}{k_{ij}^{\text{tap}}} - \dot{Z}_{kj} \dot{Y}_T^o \frac{1}{(k_{ij}^{\text{tap}})^2} \right) \frac{\partial \dot{U}_j}{\partial t_{ij}^{\text{OLTC}}} \\ & + 2\dot{Y}_T^o \Delta k_{o,ij} \frac{1}{(k_{ij}^{\text{tap}})^3} \dot{Z}_{kj} \dot{U}_j \\ & - \dot{Y}_T^o \Delta k_{o,ij} \frac{1}{(k_{ij}^{\text{tap}})^2} (\dot{Z}_{ki} \dot{U}_j + \dot{Z}_{kj} \dot{U}_i) \end{aligned} \quad (48)$$

The sensitivities of active and reactive power losses can be derived in similar ways according to [41]. Let $\boldsymbol{Y_G}$ and $\boldsymbol{Y_B}$ denote the real part and imaginary part of admittance matrix respectively, power loss sensitivities can be formulated as

$$\begin{cases} \dfrac{\partial P_{\text{loss}}}{\partial P_k} = 2\Re\left[\bar{\boldsymbol{U}}^\intercal \boldsymbol{Y_G} \dfrac{\partial \dot{\boldsymbol{U}}}{\partial P_k} \right] \\ \dfrac{\partial P_{\text{loss}}}{\partial Q_k} = 2\Re\left[\bar{\boldsymbol{U}}^\intercal \boldsymbol{Y_G} \dfrac{\partial \dot{\boldsymbol{U}}}{\partial Q_k} \right] \\ \dfrac{\partial Q_{\text{loss}}}{\partial P_k} = -2\Re\left[\bar{\boldsymbol{U}}^\intercal \boldsymbol{Y_B} \dfrac{\partial \dot{\boldsymbol{U}}}{\partial P_k} \right] \\ \dfrac{\partial Q_{\text{loss}}}{\partial Q_k} = -2\Re\left[\bar{\boldsymbol{U}}^\intercal \boldsymbol{Y_B} \dfrac{\partial \dot{\boldsymbol{U}}}{\partial Q_k} \right] \end{cases} \quad (49)$$

where $\partial\dot{\boldsymbol{U}}/\partial P_k$ and $\partial\dot{\boldsymbol{U}}/\partial Q_k$ are calculated by (30) and (46).

C. Formulation of Affine Parameterization

The detailed structures of matrices in (32), (33) and (34) are given as

$$\begin{aligned} \boldsymbol{\pi} &:= [\boldsymbol{\Delta u}(0), \ldots, \boldsymbol{\Delta u}(T-1)]^\intercal \\ \widetilde{\boldsymbol{h}} &:= [\boldsymbol{h}(0), \ldots, \boldsymbol{h}(T-1)]^\intercal \\ \boldsymbol{\omega} &:= [\boldsymbol{\Delta d}(0), \ldots, \boldsymbol{\Delta d}(T-1)]^\intercal \quad (50) \\ \boldsymbol{\Phi} &:= [\boldsymbol{x}(1), \ldots, \boldsymbol{x}(T)]^\intercal \in \mathbb{R}^{T \cdot N} \quad (51) \end{aligned}$$

$$\widetilde{\boldsymbol{M}} := \begin{bmatrix} 0 & \cdots & \cdots & 0 \\ \boldsymbol{M}_{1,0} & 0 & \cdots & 0 \\ \vdots & \ddots & \ddots & \vdots \\ \boldsymbol{M}_{T-1,0} & \cdots & \boldsymbol{M}_{T-1,T-2} & 0 \end{bmatrix} \quad (52)$$

$$\widetilde{\boldsymbol{A}} := \left[\boldsymbol{A}, \boldsymbol{A}^2, \ldots, \boldsymbol{A}^T \right]^\intercal \quad (53)$$

$$\boldsymbol{H} := \begin{bmatrix} \hat{\boldsymbol{B}} & 0 & \cdots & \cdots & 0 \\ \boldsymbol{A}\hat{\boldsymbol{B}} & \hat{\boldsymbol{B}} & 0 & \cdots & 0 \\ \boldsymbol{A}^2\hat{\boldsymbol{B}} & \boldsymbol{A}\hat{\boldsymbol{B}} & \hat{\boldsymbol{B}} & 0 & \vdots \\ \vdots & \vdots & \vdots & \ddots & \vdots \\ \boldsymbol{A}^{T-1}\hat{\boldsymbol{B}} & \boldsymbol{A}^{T-2}\hat{\boldsymbol{B}} & \cdots & \cdots & \hat{\boldsymbol{B}} \end{bmatrix} \quad (54)$$

$$\boldsymbol{L} := \begin{bmatrix} 0 & 0 & \cdots & \cdots & 0 \\ 0 & \hat{\boldsymbol{B}} & 0 & \cdots & 0 \\ 0 & \boldsymbol{A}\hat{\boldsymbol{B}} & \hat{\boldsymbol{B}} & 0 & \vdots \\ \vdots & \vdots & \vdots & \ddots & \vdots \\ 0 & \boldsymbol{A}^{T-2}\hat{\boldsymbol{B}} & \boldsymbol{A}^{T-3}\hat{\boldsymbol{B}} & \cdots & \hat{\boldsymbol{B}} \end{bmatrix} \quad (55)$$

$$\boldsymbol{E} := \begin{bmatrix} \hat{\boldsymbol{D}} & 0 & \cdots & \cdots & 0 \\ \boldsymbol{A}\hat{\boldsymbol{D}} & \hat{\boldsymbol{D}} & 0 & \cdots & 0 \\ \boldsymbol{A}^2\hat{\boldsymbol{D}} & \boldsymbol{A}\hat{\boldsymbol{D}} & \hat{\boldsymbol{D}} & 0 & \vdots \\ \vdots & \vdots & \vdots & \ddots & \vdots \\ \boldsymbol{A}^{T-1}\hat{\boldsymbol{D}} & \boldsymbol{A}^{T-2}\hat{\boldsymbol{D}} & \cdots & \cdots & \hat{\boldsymbol{D}} \end{bmatrix} \quad (56)$$

where $\boldsymbol{\pi} \in \mathbb{R}^{T \cdot U}$, $\widetilde{\boldsymbol{h}} \in \mathbb{R}^{T \cdot U}$, $\boldsymbol{\omega} \in \mathbb{R}^{T \cdot R}$, $\boldsymbol{\Phi} \in \mathbb{R}^{T \cdot N}$, $\widetilde{\boldsymbol{M}} \in \mathbb{R}^{T \cdot U \times T \cdot R}$, $\widetilde{\boldsymbol{A}} \in \mathbb{R}^{T \cdot N \times N}$, $\boldsymbol{H} \in \mathbb{R}^{T \cdot N \times T \cdot U}$, $\boldsymbol{L} \in \mathbb{R}^{T \cdot N \times T \cdot U}$, $\boldsymbol{E} \in \mathbb{R}^{T \cdot N \times T \cdot R}$; $\boldsymbol{\pi}$, $\boldsymbol{\omega}$, $\widetilde{\boldsymbol{h}}$ and $\widetilde{\boldsymbol{M}}$ are extensions of $\boldsymbol{\Delta u}$, $\boldsymbol{\Delta d}$, $\boldsymbol{h}$ and $\boldsymbol{M}$ respectively; $\boldsymbol{\Phi}$ is a column vector containing nodal

voltage magnitudes at each time instant; $\boldsymbol{A}$ is the identity matrix; $\hat{\boldsymbol{B}}$ and $\hat{\boldsymbol{D}}$ are sensitivity matrices in the state space model in (18).

ACKNOWLEDGMENT

The authors would like to express sincere appreciation to the editor and the reviewers for their constructive comments and suggestions on improving the quality of this paper.

REFERENCES

[1] C. Wan, J. Lin, W. Guo, and Y. Song, "Maximum uncertainty boundary of volatile distributed generation in active distribution network," *IEEE Trans. Smart Grid*, vol. 9, no. 4, pp. 2930–2942, Jul. 2018.
[2] S. Bahrami, M. H. Amini, M. Shafie-Khah, and J. P. Catalao, "A decentralized renewable generation management and demand response in power distribution networks," *IEEE Trans. Sustain. Energy*, vol. 9, no. 4, pp. 1783–1797, Oct. 2018.
[3] B.-M. Hodge *et al.*, "Wind power forecasting error distributions: An international comparison," in *Proc. 11th Annu. Int. Workshop Large-Scale Integr. Wind Power Power Syst./Transmiss. Netw. Offshore Wind Power Plants Conf.*, 2012, pp. 2–4.
[4] C. D'Adamo, S. Jupe, and C. Abbey, "Global survey on planning and operation of active distribution networks—Update of CIGRE C6.11 working group activities," in *Proc. Int. Conf. Exhib. Elect. Distrib.*, 2009, pp. 1–4.
[5] J. McDonald, "Adaptive intelligent power systems: Active distribution networks," *Energy Policy*, vol. 36, no. 12, pp. 4346–4351, 2008.
[6] C. Wan, Z. Xu, P. Pinson, Z. Y. Dong, and K. P. Wong, "Optimal prediction intervals of wind power generation," *IEEE Trans. Power Syst.*, vol. 29, no. 3, pp. 1166–1174, May 2014.
[7] F. Capitanescu, I. Bilibin, and E. R. Ramos, "A comprehensive centralized approach for voltage constraints management in active distribution grid," *IEEE Trans. Power Syst.*, vol. 29, no. 2, pp. 933–942, Mar. 2014.
[8] Q. Zhou and J. Bialek, "Generation curtailment to manage voltage constraints in distribution networks," *IET Gener., Transmiss. Distrib.*, vol. 1, no. 3, pp. 492–498, May 2007.
[9] H.-G. Yeh, D. F. Gayme, and S. H. Low, "Adaptive VAR control for distribution circuits with photovoltaic generators," *IEEE Trans. Power Syst.*, vol. 27, no. 3, pp. 1656–1663, Aug. 2012.
[10] C. Wan, J. Lin, J. Wang, Y. Song, and Z. Y. Dong, "Direct quantile regression for nonparametric probabilistic forecasting of wind power generation," *IEEE Trans. Power Syst.*, vol. 32, no. 4, pp. 2767–2778, Jul. 2017.
[11] C. E. Garcia, D. M. Prett, and M. Morari, "Model predictive control: theory and practice-a survey," *Automatica*, vol. 25, no. 3, pp. 335–348, 1989.
[12] G. Valverde and T. Van Cutsem, "Model predictive control of voltages in active distribution networks," *IEEE Trans. Smart Grid*, vol. 4, no. 4, pp. 2152–2161, Dec. 2013.
[13] X. Xing, J. Lin, C. Wan, and Y. Song, "Model predictive control of LPC-looped active distribution network with high penetration of distributed generation," *IEEE Trans. Sustain. Energy*, vol. 8, no. 3, pp. 1051–1063, Jul. 2017.
[14] H. S. Bidgoli and T. H. V. Cutsem, "Combined local and centralized voltage control in active distribution networks," *IEEE Trans. Power Syst.*, vol. 33, no. 2, pp. 1374–1384, Mar. 2018.
[15] S. Gill, I. Kockar, and G. W. Ault, "Dynamic optimal power flow for active distribution networks," *IEEE Trans. Power Syst.*, vol. 29, no. 1, pp. 121–131, Jan. 2014.
[16] M. F. Shaaban, M. Ismail, E. F. El-Saadany, and W. Zhuang, "Real-time PEV charging/discharging coordination in smart distribution systems," *IEEE Trans. Smart Grid*, vol. 5, no. 4, pp. 1797–1807, Jul. 2014.
[17] J. A. Pinzon, P. P. Vergara, L. C. da Silva, and M. J. Rider, "Optimal management of energy consumption and comfort for smart buildings operating in a microgrid," *IEEE Trans. Smart Grid*, 2018, to be published, doi: 10.1109/TSG.2018.2822276.
[18] C. Wan, J. Lin, Y. Song, Z. Xu, and G. Yang, "Probabilistic forecasting of photovoltaic generation: An efficient statistical approach," *IEEE Trans. Power Syst.*, vol. 32, no. 3, pp. 2471–2472, May 2017.
[19] J. C. Smith, G. Hensley, and L. Ray, *IEEE Recommended Practice for Monitoring Electric Power Quality*, IEEE Std 1159-2009, 1995.
[20] F. Luo, W. Wei, C. Wang, J. Huang, Q. Yin, and Y. Bai, "Research and application of GIS-based medium-voltage distribution network comprehensive technical evaluation system," *Int. Trans. Elect. Energy Syst.*, vol. 25, no. 11, pp. 2674–2684, 2015.
[21] D. Zhu and G. Hug, "Decomposed stochastic model predictive control for optimal dispatch of storage and generation," *IEEE Trans. Smart Grid*, vol. 5, no. 4, pp. 2044–2053, Jul. 2014.
[22] S. R. Cominesi, M. Farina, L. Giulioni, B. Picasso, and R. Scattolini, "A two-layer stochastic model predictive control scheme for microgrids," *IEEE Trans. Control Syst. Technol.*, vol. 26, no. 1, pp. 1–13, Jan. 2018.
[23] R. E. Griffith and R. Stewart, "A nonlinear programming technique for the optimization of continuous processing systems," *Manage. Sci.*, vol. 7, no. 4, pp. 379–392, 1961.
[24] Q. Zhou and J. Bialek, "Simplified calculation of voltage and loss sensitivity factors in distribution networks," in *Proc. 16th Power Syst. Comput. Conf.*, 2008, pp. 1–6.
[25] E. DallAnese, K. Baker, and T. Summers, "Chance-constrained AC optimal power flow for distribution systems with renewables," *IEEE Trans. Power Syst.*, vol. 32, no. 5, pp. 3427–3438, Sep. 2017.
[26] D. Bienstock, M. Chertkov, and S. Harnett, "Chance-constrained optimal power flow: Risk-aware network control under uncertainty," *Siam Rev.*, vol. 56, no. 3, pp. 461–495, 2014.
[27] A. Venzke, L. Halilbasic, U. Markovic, G. Hug, and S. Chatzivasileiadis, "Convex relaxations of chance constrained AC optimal power flow," *IEEE Trans. Power Syst.*, vol. 33, no. 3, pp. 2829–2841, May 2018.
[28] Q. Wang, Y. Guan, and J. Wang, "A chance-constrained two-stage stochastic program for unit commitment with uncertain wind power output," *IEEE Trans. Power Syst.*, vol. 27, no. 1, pp. 206–215, Feb. 2012.
[29] M. D. Tabone and D. S. Callaway, "Modeling variability and uncertainty of photovoltaic generation: A hidden state spatial statistical approach," *IEEE Trans. Power Syst.*, vol. 30, no. 6, pp. 2965–2973, Nov. 2015.
[30] C. Wan, Z. Xu, P. Pinson, Z. Y. Dong, and K. P. Wong, "Probabilistic forecasting of wind power generation using extreme learning machine," *IEEE Trans. Power Syst.*, vol. 29, no. 3, pp. 1033–1044, May 2014.
[31] Q. Wang, J. Wang, and Y. Guan, "Stochastic unit commitment with uncertain demand response," *IEEE Trans. Power Syst.*, vol. 28, no. 1, pp. 562–563, Feb. 2013.
[32] M. Liu, C. A. Canizares, and W. Huang, "Reactive power and voltage control in distribution systems with limited switching operations," *IEEE Trans. Power Syst.*, vol. 24, no. 2, pp. 889–899, May 2009.
[33] I. Džafić, R. A. Jabr, E. Halilovic, and B. C. Pal, "A sensitivity approach to model local voltage controllers in distribution networks," *IEEE Trans. Power Syst.*, vol. 29, no. 3, pp. 1419–1428, May 2014.
[34] F. Oldewurtel, C. N. Jones, and M. Morari, "A tractable approximation of chance constrained stochastic MPC based on affine disturbance feedback," in *Proc. 47th IEEE Conf. Decis. Control*, 2008, pp. 4731–4736.
[35] A. Mesbah, "Stochastic model predictive control: An overview and perspectives for future research," *IEEE Control Syst.*, vol. 36, no. 6, pp. 30–44, Dec. 2016.
[36] A. Shapiro, D. Dentcheva, and A. Ruszczyński, *Lectures on Stochastic Programming: Modeling and Theory*. Philadelphia, PA, USA: SIAM, 2009.
[37] S. H. Low, "Convex relaxation of optimal power flow—part I: Formulations and equivalence," *IEEE Trans. Control Netw. Syst.*, vol. 1, no. 1, pp. 15–27, Mar. 2014.
[38] R. A. Jabr, "Radial distribution load flow using conic programming," *IEEE Trans. Power Syst.*, vol. 21, no. 3, pp. 1458–1459, Aug. 2006.
[39] M. E. Baran and F. F. Wu, "Network reconfiguration in distribution systems for loss reduction and load balancing," *IEEE Trans. Power Del.*, vol. PWRD-4, no. 2, pp. 1401–1407, Apr. 1989.
[40] W. H. Kersting, "Radial distribution test feeders," in *Proc. Power Eng. Soc. Winter Meeting*, 2001, vol. 2, pp. 908–912.
[41] A. J. Conejo, F. D. Galiana, and I. Kockar, "Z-bus loss allocation," *IEEE Trans. Power Syst.*, vol. 16, no. 1, pp. 105–110, Feb. 2001.

Yibao Jiang received the B.S. degree in 2015 from Zhejiang University, Hangzhou, China, where he is currently working toward the Ph.D. degree with the College of Electrical Engineering.

He works with the Smart Grid Operation and Optimization Laboratory, College of Electrical Engineering, Zhejiang University, as a Research Assistant. He also holds a Visiting Graduate position with the Laboratory for Information and Decision Systems, Massachusetts Institute of Technology, Cambridge, MA, USA. His research interests include optimization and control of distribution systems and multi-energy systems.

Can Wan (M'15) received the B.Eng. degree from Zhejiang University, Hangzhou, China, in 2008, and the Ph.D. degree from The Hong Kong Polytechnic University, Hong Kong, in 2015.

He is a Research Professor with the College of Electrical Engineering, Zhejiang University, Hangzhou, China, under the University Hundred Talents Program. He was a Postdoc Fellow with the Department of Electrical Engineering, Tsinghua University, Beijing, China, and held research positions at Technical University of Denmark, The Hong Kong Polytechnic University, and City University of Hong Kong. He was a Visiting Scholar with the Center for Electric Power and Energy, Technical University of Denmark, and Argonne National Laboratory, Lemont, IL, USA. His research interests include forecasting, renewable energy, active distribution network, integrated energy systems, and machine learning.

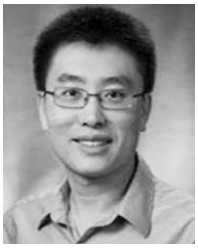

Jianhui Wang (M'07–SM'12) received the Ph.D. degree in electrical engineering from Illinois Institute of Technology, Chicago, IL, USA, in 2007.

He is currently an Associate Professor with the Department of Electrical Engineering, Southern Methodist University (SMU), Dallas, TX, USA. Prior to joining SMU, he had an 11-year stint at Argonne National Laboratory with the last appointment as Section Lead Advanced Grid Modeling.

Dr. Wang is the Secretary of the IEEE Power and Energy Society (PES) Power System Operations, Planning and Economics Committee. He has held visiting positions in Europe, Australia, and Hong Kong including a VELUX Visiting Professorship at the Technical University of Denmark. He is the Editor-in-Chief for the IEEE TRANSACTIONS ON SMART GRID and an IEEE PES Distinguished Lecturer. He is also the recipient of the IEEE PES Power System Operation Committee Prize Paper Award in 2015.

Yonghua Song (M'90–SM'94–F'08) received the B.Eng. degree from Chengdu University of Science and Technology, Chengdu, China, in 1984, and the Ph.D. degree from China Electric Power Research Institute, Beijing, China, in 1989.

He is currently a Rector with Macau University, Macau, China, and also an Adjunct Professor with the College of Electrical Engineering, Zhejiang University, Hangzhou, China. From 2012 to 2017, he was the Executive Vice-President with Zhejiang University. From 1989 to 1991, he was a Postdoctoral Fellow with Tsinghua University, Beijing, China. He then held various positions with Bristol University, Bristol, U.K.; Bath University, Bath, U.K.; and John Moores University, Liverpool, U.K., from 1991 to 1996. In 1997, he was a Professor of power systems with Brunel University, Uxbridge, U.K., where he has been the Pro-Vice Chancellor of graduate studies since 2004. In 2007, he took up the Pro-Vice Chancellorship and Professorship of Electrical Engineering with the University of Liverpool, Liverpool, U.K. He was a Professor with the Department of Electrical Engineering, Tsinghua University, where he was an Assistant President and the Deputy Director with the Laboratory of Low-Carbon Energy in 2009. His current research interests include smart grid, electricity economics, and operation and control of power systems.

Prof. Song was a recipient of the D.Sc. Award from Brunel University in 2002 for his original achievements in power systems research. He was elected Vice-President of the Chinese Society for Electrical Engineering (CSEE) and appointed Chairman of the International Affairs Committee of the CSEE in 2009. In 2004, he was elected as a fellow of the Royal Academy of Engineering, U.K.

Zhao Yang Dong (M'99–SM'06–F'16) received the Ph.D. degree from the University of Sydney, NSW, Australia, in 1999.

He is currently a Professor with the School of Electrical Engineering and Telecommunications, University of New South Wales, Sydney, NSW, Australia. During 2013–2017, he served as the Head of the School of Electrical and Information Engineering, University of Sydney. He is an immediate Ausgrid Chair Professor and the Director of the Centre for Intelligent Electricity Networks, University of Newcastle, Australia. His research interests include smart grid, power system planning, power system security, load modeling, renewable energy systems, electricity market, and computational intelligence and its application in power engineering.

Prof. Dong is an Editor for the IEEE TRANSACTIONS ON SMART GRID, the IEEE POWER ENGINEERING LETTERS, and the IEEE TRANSACTIONS ON SUSTAINABLE ENERGY.